Rapid attribution analysis of the extraordinary heatwave on the Pacific Coast of the US and Canada June 2021.

Contributors

Sjoukje Y. Philip[1], Sarah F. Kew[1], Geert Jan van Oldenborgh[1,19], Wenchang Yang[2], Gabriel A. Vecchi[2,3], Faron S. Anslow[4], Sihan Li[5], Sonia I. Seneviratne[6], Linh N. Luu[1], Julie Arrighi[7,8,9], Roop Singh[7], Maarten van Aalst[7,8,10], Mathias Hauser[6], Dominik L. Schumacher[6], Carolina Pereira Marghidan[8], Kristie L Ebi[11], Rémy Bonnet[12], Robert Vautard[12], Jordis Tradowsky[13,14], Dim Coumou[1, 15], Flavio Lehner[16,17], Michael Wehner[18], Chris Rodell[20], Roland Stull[20], Rosie Howard[20], Nathan Gillett[21], Friederike E L Otto[5]

[1] Royal Netherlands Meteorological Institute (KNMI), De Bilt, The Netherlands
[2] Department of Geosciences, Princeton University, Princeton, 08544, USA
[3]The High Meadows Environmental Institute, Princeton University, Princeton, 08544, USA
[4]Pacific Climate Impacts Consortium, University of VIctoria, Victoria, V8R4J1, Canada
[5] School of Geography and the Environment, University of Oxford, UK
[6] Institute for Atmospheric and Climate Science, Department of Environmental Systems Science, ETH Zurich, Zurich, Switzerland
[7] Red Cross Red Crescent Climate Centre, The Hague, the Netherlands
[8] Faculty of Geo-Information Science and Earth Observation (ITC), University of Twente, Enschede, the Netherlands
[9] Global Disaster Preparedness Center, American Red Cross, Washington DC, USA
[10] International Research Institute for Climate and Society, Columbia University, New York, USA
[11] Center for Health and the Global Environment, University of Washington, Seattle WA USA
[12] Institut Pierre-Simon Laplace, CNRS, Sorbonne Université, Paris, France
[13] Deutscher Wetterdienst, Regionales Klimabüro Potsdam, Potsdam, Germany
[14] Bodeker Scientific, Alexandra, New Zealand
[15] Institute for Environmental Studies (IVM), VU Amsterdam, The Netherlands
[16] Department of Earth and Atmospheric Sciences, Cornell University, USA
[17] Climate and Global Dynamics Laboratory, National Center for Atmospheric Research, USA
[18] Lawrence Berkeley National Laboratory, Berkeley, California USA
[19] Atmospheric, Oceanic and Planetary Physics, University of Oxford, UK
[20]Department of Earth, Ocean, and Atmospheric Sciences, The University of British Columbia, Vancouver, V6T1Z4, Canada
[21]Canadian Centre for Climate Modelling and Analysis, Environment and Climate Change Canada, Victoria, BC, Canada.

Main findings

- Based on observations and modeling, the occurrence of a heatwave with maximum daily temperatures (TXx) as observed in the area 45–52 ºN, 119–123 ºW, was virtually impossible without human-caused climate change.
- The observed temperatures were so extreme that they lie far outside the range of historically observed temperatures. This makes it hard to quantify with confidence how rare the event was. In the most realistic statistical analysis the event is estimated to be about a 1 in 1000 year event in today's climate.

- There are two possible sources of this extreme jump in peak temperatures. The first is that this is a very low probability event, even in the current climate which already includes about 1.2°C of global warming -- the statistical equivalent of really bad luck, albeit aggravated by climate change. The second option is that nonlinear interactions in the climate have substantially increased the probability of such extreme heat, much beyond the gradual increase in heat extremes that has been observed up to now. We need to investigate the second possibility further, although we note the climate models do not show it. All numbers below assume that the heatwave was a very low probability event that was not caused by new nonlinearities.
- With this assumption and combining the results from the analysis of climate models and weather observations, an event, defined as daily maximum temperatures (TXx) in the heatwave region, as rare as 1 in a 1000 years would have been at least 150 times rarer without human-induced climate change.
- Also, this heatwave was about 2°C hotter than it would have been if it had occurred at the beginning of the industrial revolution (when global mean temperatures were 1.2°C cooler than today).
- Looking into the future, in a world with 2°C of global warming (0.8°C warmer than today which at current emission levels would be reached as early as the 2040s), this event would have been another degree hotter. An event like this -- currently estimated to occur only once every 1000 years, would occur roughly every 5 to 10 years in that future world with 2°C of global warming.

In summary, an event such as the Pacific Northwest 2021 heatwave is still rare or extremely rare in today's climate, yet would be virtually impossible without human-caused climate change. As warming continues, it will become a lot less rare.

Our results provide a strong warning: our rapidly warming climate is bringing us into uncharted territory that has significant consequences for health, well-being, and livelihoods. Adaptation and mitigation are urgently needed to prepare societies for a very different future. Adaptation measures need to be much more ambitious and take account of the rising risk of heatwaves around the world, including surprises such as this unexpected extreme. Deaths from extreme heat can be dramatically reduced with adequate preparedness action. Heat action plans that incorporate heatwave early warning systems can strengthen the resilience of cities and people. In addition, longer-term plans are needed to modify our built environments to be more adequate for the hotter climate that we already experience today and the additional warming that we expect in future. In addition, greenhouse gas mitigation goals should take into account the increasing risks

associated with unprecedented climate conditions if warming would be allowed to continue

1 Introduction

During the last days of June 2021, Pacific northwest areas of the U.S. and Canada experienced temperatures never previously observed, with records broken in multiple cities by several degrees Celsius. Temperatures far above 40 ºC (104 ºF) occurred on Sunday 27 to Tuesday 29 June (Figs 1a,b for Monday) in the Pacific northwest areas of the U.S. and western Provinces of Canada, with the maximum warmth moving from the western to the eastern part of the domain from Monday to Tuesday. The anomalies relative to normal maximum temperatures for the time of year reached 16°C to 20 ºC (Figs 1c,d). It is noteworthy that these record temperatures occurred one whole month before the climatologically warmest part of the year (end of July, early August), making them particularly exceptional. Even compared to the maximum temperatures in other years independent of the considered month, the recent event exceeds those temperatures by about 5 ºC (Figure 2). Records were shattered in a very large area, including setting a new all-time Canadian temperature record in the village of Lytton, at which a temperature of 49.6 ºC was measured on June 29[1,2,3,4], and where wildfires spread on the following day[3]

[1] https://public.wmo.int/en/media/news/june-ends-exceptional-heat
[2] https://www.cbc.ca/news/canada/british-columbia/canada-bc-alberta-heat-wave-heat-dome-temperature-records-1.6084203
[3] https://www.cbc.ca/news/canada/british-columbia/bc-wildfires-june-30-2021-1.6085919
[4] https://www.reuters.com/business/environment/wildfire-forces-evacuation-residents-small-western-canada-town-2021-07-01/

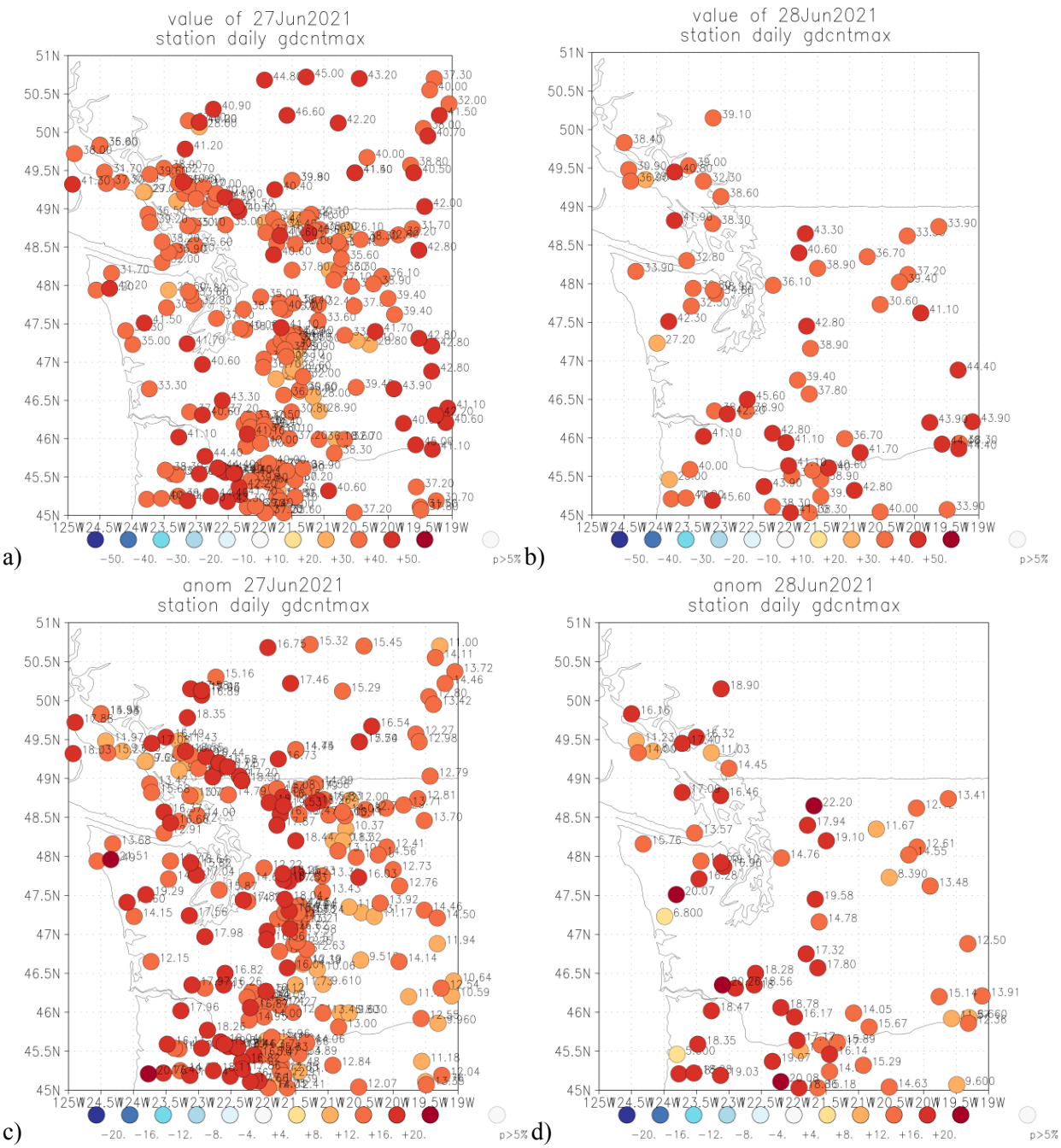

Figure 1. a) observed temperatures on 27 June 2021, b) 28 June 2021, c,d) same for anomalies relative to the whole station records.

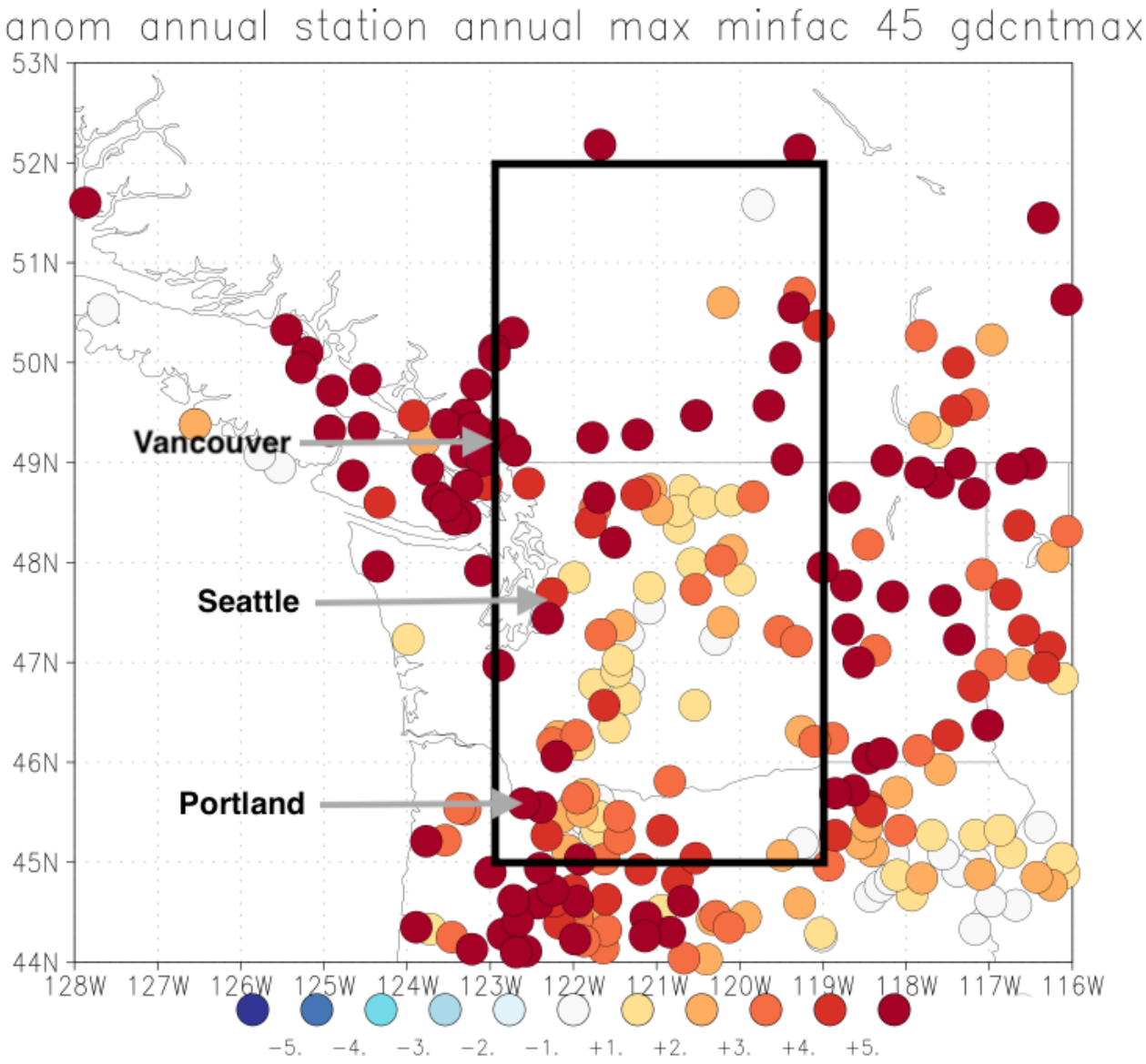

Figure 2. Anomalies of 2021 highest daily maximum temperature (TXx) relative to the whole time series, assuming the rest of the summer is cooler than this heatwave. Note that some stations do not have data up to the peak of the heatwave yet and hence underestimate the event. Negative values certainly do not include the heatwave and have therefore been deleted. The black box indicates the study region. Source: GHCN-D downloaded 4 July 2021.

Given that the observed temperatures were so far outside historical experiences and in a region with only about 50% household air conditioning penetration, we expect large impacts on health. The excess deaths numbers will only be available in 3–6 months (Canada) or a year (US), but preliminary indications from Canada are that it has already caused at least several hundreds of extra deaths[5,6].

[5] https://www.bbc.com/news/world-us-canada-57668738
[6] https://www.washingtonpost.com/world/2021/06/29/canada-heat-dome-deaths/

The present report aims to investigate the role of human-induced climate change in the likelihood and intensity of this extreme heatwave, following the established methods of multi-model multi-method approach of extreme event attribution (Philip et al., 2020; van Oldenborgh et al., 2021). We focus the analysis on the maximum temperatures in the region where most people have been affected by the heat (45 °N–52 ºN, 119 °W–123 ºW) including the cities of Seattle, Portland, and Vancouver. While the extreme heat was an important driver of the observed impacts, it is important to highlight that the meteorological extremes assessed here only partly represent one component of these described impacts, the hazard, whereas the impacts strongly depend on exposure and vulnerability too, as well as other climatological components of the hazard. In addition to the attribution of the extreme temperatures we qualitatively assess whether meteorological drivers and antecedent conditions played an important role in the observed extreme temperatures in section 7.

1.1 Event definition

Daily maximum temperatures were the headline figure in the large number of media reports describing the heatwave and the impacts associated with the event. Furthermore, daily maximum temperature was the primary extreme characteristic of the event. We therefore defined the event based on the annual maximum of daily maximum temperature, TXx. There is some evidence that longer time scales, e.g. 3-day average, better describe the health impacts (e.g., D'Ippoliti et al, 2010). However, TXx is a standard heat impact index and thus the results can easily be compared to other studies. High minimum temperatures also have strong impacts on human health. However, here we intentionally focus on one event definition to keep this rapid analysis succinct, choosing TXx, which not only characterises the extreme character of the event but is also readily available in climate models allowing us to use a large range of different models.

As the spatial scale of the event we consider the area 45°N-52°N, 119°W-123°W. This covers the more populated region around Portland, Seattle and Vancouver that were impacted heavily by the heat (with a total population of over 9.4 million in their combined metropolitan areas), but excludes the rainforest to the west and arid areas to the east. Note that this spatial event definition is based on the expected and reported human impacts rather than on the meteorological extremity. Besides this main definition we also analysed the observations for three stations in Portland, Seattle and Vancouver with long homogeneous time series.

1.2 Previous trends in heatwaves

Figure 3 shows the observed trends in TXx in the GHCN-D dataset over 1900–2019. The stations were selected on the basis of long time series, at least 50 years of data, and being at least 2º apart. The trend is defined as the regression on the global mean temperature, so the numbers represent how much slower or faster than the global mean the temperature has changed. Individual stations with different trends than nearby stations usually have inhomogeneities in the observational method or local environment.The negative trends in eastern North America and parts of California are well-understood to be the result of land use changes, irrigation and changes in agricultural practice (Cook et al., 2011; Donat et al., 2016, 2017; Thiery et al., 2017, Cowan et al., 2020). The large trends in heatwaves in Europe are not yet understood (Vautard et al, 2020). The Pacific Northwest showed trends of about two times the global temperature trend up to 2019.

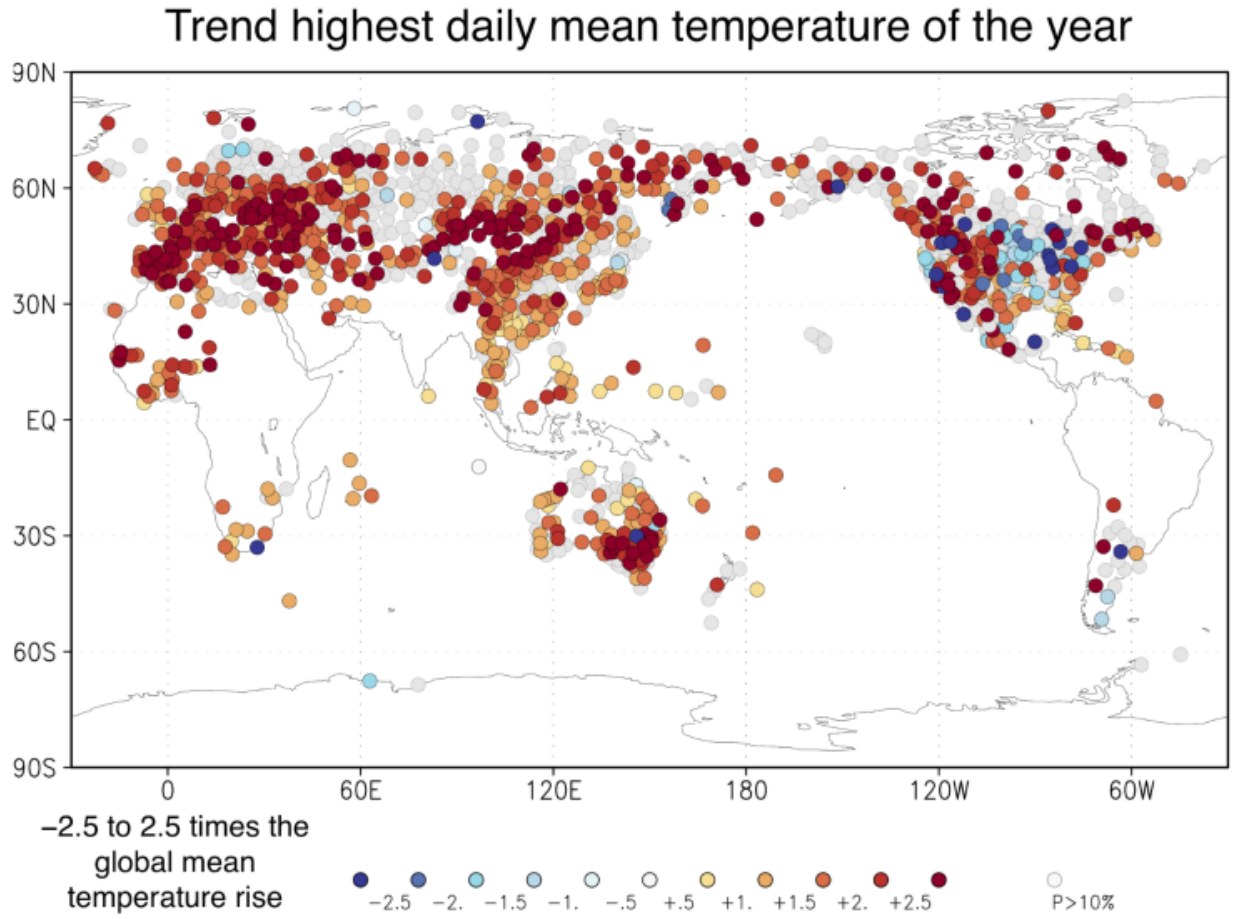

Figure 3. Trends in the highest daily maximum temperature of the year in the GHCN-D station data. Stations are selected to have at least 50 years of data and at least 2° apart. The trend is defined by the regression on the global mean temperature.

2 Data and methods

2.1 Observational data

The main dataset used to represent the heatwave is the ERA5 reanalysis (Hersbach et al., 2020), extended to the time of the heatwave by ECMWF operational analyses produced using a later version of the same model. All fields were downloaded at 0.25º resolution from the ECMWF. Both products are the optimal combination of observations, including near-surface temperature observations from meteorological stations, and the high-resolution ECMWF weather forecast model IFS. Due to the constraints of the surface temperature observations, we expect no large biases between the main dataset and the extension, although some differences may be possible under these extreme conditions.

Temperature observations were collected to directly assess the probability ratios and return periods associated with the event for the three major cities in the study area; Portland, Seattle, and Vancouver. Observing sites were chosen that had long homogenized historical records and were representative of the

severity of the event by avoiding exposure to nearby large water bodies. Sites were also chosen to be representative of the populous areas of each city to better illuminate impact on inhabitants.

For Portland, the Portland International Airport National Weather Service station was used, which has continuous observations over 1938–2021. The airport is located close to the city centre, adjacent to the Columbia River. The river's influence is thought to be small and the water temperature is warm by June. For Seattle, Seattle-Tacoma International Airport was chosen, which has almost continuous observations 1948–2021, among the longest records in the Seattle area. This location is further inland and lacks the influence of Lake Washington that downtown Seattle has. Two long records exist adjacent to downtown Vancouver, but they are both very exposed to the Georgia Strait that influenced observations due to local onshore flow during the peak of the event. A record was chosen further inland at New Westminster. The observations start in 1875 but here are data gaps 1882–1893, 1928, 1980–1993.

The data for Portland International Airport and Seattle-Tacoma International Airport were gathered from the Global Historical Climatology Network Daily (GHCN-D; Menne et al., 2012) while data for New Westminster were gathered from the Adjusted Homogenized Canadian Climate Dataset (AHCCD) for daily temperature (Vincent et al., 2020). The AHCCD dataset is updated annually and ends in 2020. Data for 2021 were appended from unhomogenized recent records from Environment and Climate Change Canada. Overlapping data for 2020 were compared between the two sources and found to be identical except several duplicate/missing observations which would not cause error in the present analysis because the records are complete for June, 2021.

As a measure of anthropogenic climate change we use the global mean surface temperature (GMST), where GMST is taken from the National Aeronautics and Space Administration (NASA) Goddard Institute for Space Science (GISS) surface temperature analysis (GISTEMP, Hansen et al., 2010 and Lenssen et al. 2019). We apply a 4-yr running mean low-pass filter to suppress the influence of ENSO and winter variability at high northern latitudes as these are unforced variations.

2.2 Model and experiment descriptions

Model simulations from the 6th Coupled Model Intercomparison Project (CMIP6; Eyring et al., 2016) are assessed. We combine the historical simulations (1850 to 2015) with the Shared Socioeconomic Pathway (SSP) projections (O'Neill et al., 2016) for the years 2016 to 2100. Here, we only use data from SSP5-8.5, although the pathways are very similar to each other over the period 2015–2021. Models are excluded if they do not provide the relevant variables, do not run from 1850 to 2100, or include duplicate time steps or missing time steps. All available ensemble members are used. A total of 18 models (88 ensemble members), which fulfill these criteria and passed the validation tests (Section 4), are used.

In addition to the CMIP6 simulations, the ensemble of extended historical simulations from the IPSL-CM6A-LR model is used (see Boucher et al., 2020 for a description of the model). It is composed of 32 members, following the CMIP6 protocol (Eyring et al., 2016) over the historical period (1850-2014) and extended until 2029 using all forcings from the SSP2-4.5 scenario, except for the ozone concentration which has been kept constant at its 2014 climatology (as it was not available at the time of performing the extensions). This ensemble is used to explore the influence of internal variability.

The GFDL-CM2.5/FLOR (Vecchi et al., 2014) is a fully coupled climate model developed at the Geophysical Fluid Dynamics Laboratory (GFDL). While the ocean and ice components have a horizontal resolution of only 1 degree, the resolution of the atmosphere and land is about 50 km and therefore might provide a better simulation of certain extreme weather events (Baldwin et al. 2019). The data used in this study cover the period from 1860 to 2100, and include both the historical and RCP4.5 experiments driven by transient radiative forcings from CMIP5 (Taylor et al., 2012).

We also examine five ensemble members of the AMIP experiment (1871-2019) from the GFDL-AM2.5C360 (Yang et al. 2021, Chan et al. 2021), which consists of the atmosphere and land components of the FLOR model but with horizontal resolution doubled to 25 km for a potentially better representation of extreme events.

The Climate of the 20th Century Plus project (C20C+) was designed specifically for event attribution studies (Stone et al. 2019). The experimental design uses models of the atmosphere and land with prescribed sea surface temperatures and sea ice concentrations, similar to the AMIP experiment. To quantify the impact, if any, on extreme events, participating models were run in two configurations. The first followed AMIP protocols to represent the actual world — "world as it was". The second represented a counterfactual "world that might have been" without the anthropogenic climate by suitably altering the prescribed sea surface temperature and ice boundary conditions as well as atmospheric trace gas compositions. The distributions of TXx in the study area were examined in three C20C+ models, CAM5.1, MIROC5 and HadGEM3-A-N216 and compared to that of the ERA5 reanalysis. Only the Community Atmospheric Model (CAM5.1), run at the default ~1° resolution, satisfied the requirements of this study in the statistical description of heat extremes. The model is described in Neale et al. (2010). The actual world ensemble consists of 99 simulations of mixed duration all ending in 2018 resulting in a sample size of 4090 years. A counterfactual world ensemble of similar size consists of 89 simulations resulting in a sample size of 3823 years.

2.3 Statistical methods

A full description of the statistical methods is given in Philip et al (2020) and van Oldenborgh et al (2021). Here we give a summary.

As discussed in section 1.2, we analyse the annual maximum of daily maximum temperatures (TXx) averaged over 45°N-52°N, 119°W-123°W. Initially, we analyse reanalysis data and station data from sites with long records. Next, we analyse climate model output for the same metric. We follow the steps outlined in the WWA protocol for event attribution. The analysis steps include: (i) trend calculation from observations; (ii) model validation; (iii) multi-method multi-model attribution and (iv) synthesis of the attribution statement.

For the event under investigation we calculate the return periods, probability ratio (PR) and change in intensity as a function of GMST. The two climates we compared are defined as the current 2021 event and a GMST value representative of the climate of late nineteenth century, −1.2 ºC relative to 2021 (1850-1900, based on the Global Warming Index https://www.globalwarmingindex.org). To statistically model the selected event, we use a GEV distribution that shifts with GMST, i.e., the location parameter has a term proportional to GMST and the scale and shape parameters are assumed constant. Next, results

from observations and from the models are synthesized into a consistent attribution statement. For models (except for IPSL-CM6A-LR and CAM5.1), we additionally analyse the PR between a future climate at +2°C above the 1850-1900 reference, which is equivalent to +0.8°C above the current climate of 2021. For this analysis we use model data up to about 2050 or when the model GMST reaches +0.8 ºC compared to now.

The CMIP6 data are analysed using the same statistical models as the main method. However, the parameter uncertainty is estimated in a Bayesian setting using a Markov Chain Monte Carlo (MCMC) sampler instead of a bootstrapping approach.

3 Observational analysis: return time and trend

Time series of various aspects of the main index are shown in Figure 4: a) the last 90 days combined from ERA5 up to 30 May, ECMWF analyses up to 29 June, ECMWF forecast up to 7 July; and b) annual max of the series. The value for 2021, 39.5 ºC, is 5.5 ºC above the previous record of 34.0 ºC, which is an extremely large increase that gives rise to difficulties in the statistical analysis described in Section 3.1.

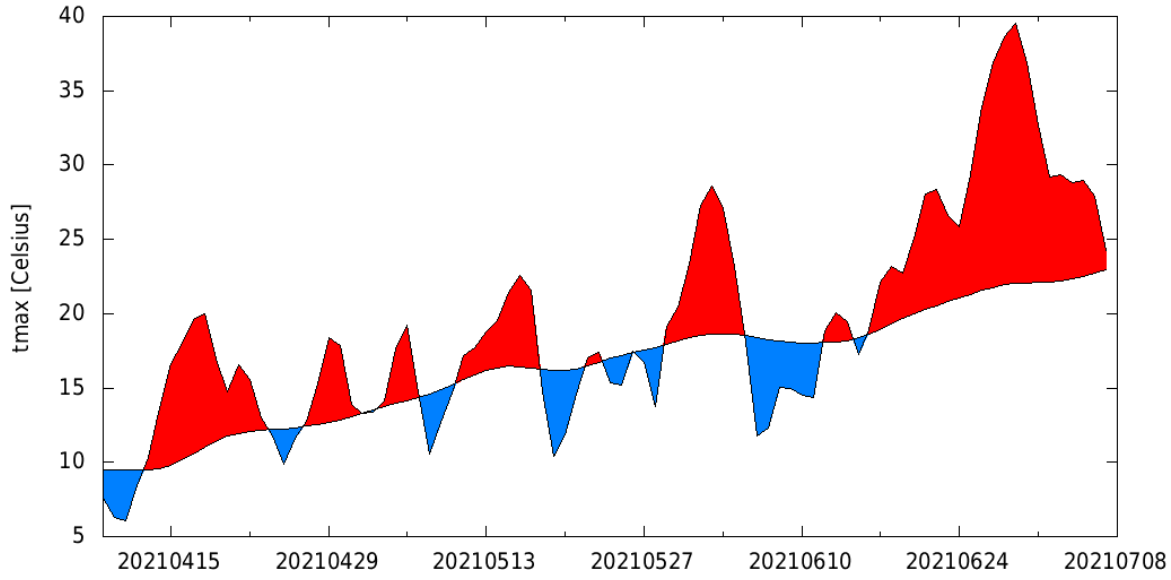

a)

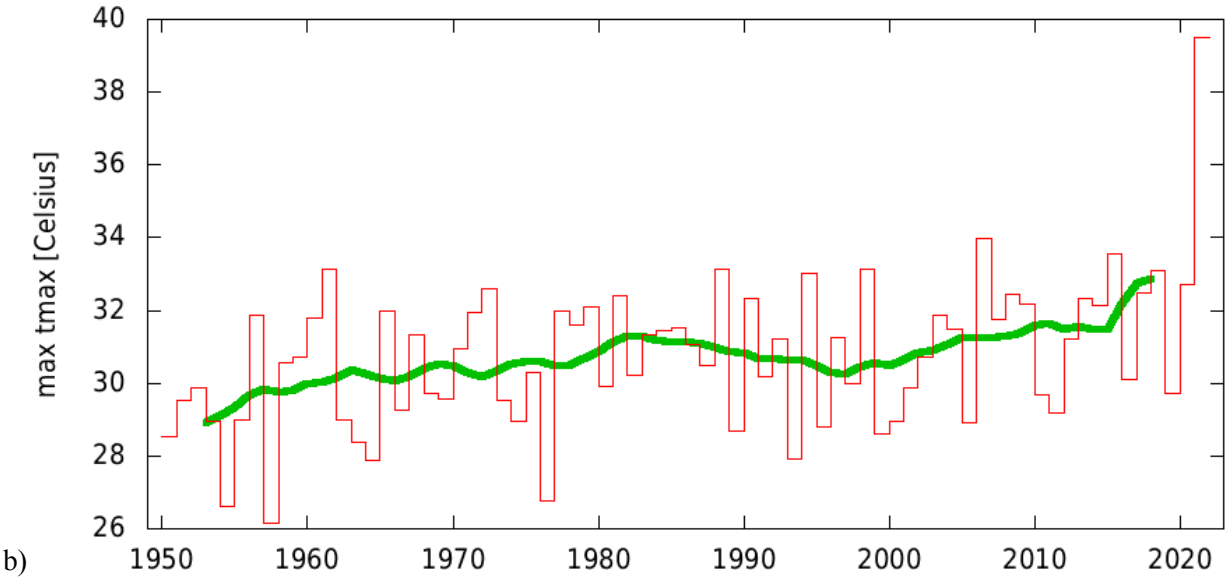

Figure 4. a) Last 90 days of the average temperature over the study area based on ERA5 (up to 30 May 2021), ECMWF analyses (up to 29 June 2021) and forecasts (up to 7 July 2021), with positive and negative departures from the 1991–2020 climatological mean of daily maximum temperature shaded red and blue, respectively. b) Annual maximum of the index series with a 10-yr running mean (green line).

In Figure 5a we show the seasonal cycle of the daily maximum temperature averaged over the index region and in Figure 5b the spatial pattern of the annual maximum of the daily maximum temperature at each grid point. These are also used in the model validation procedure.

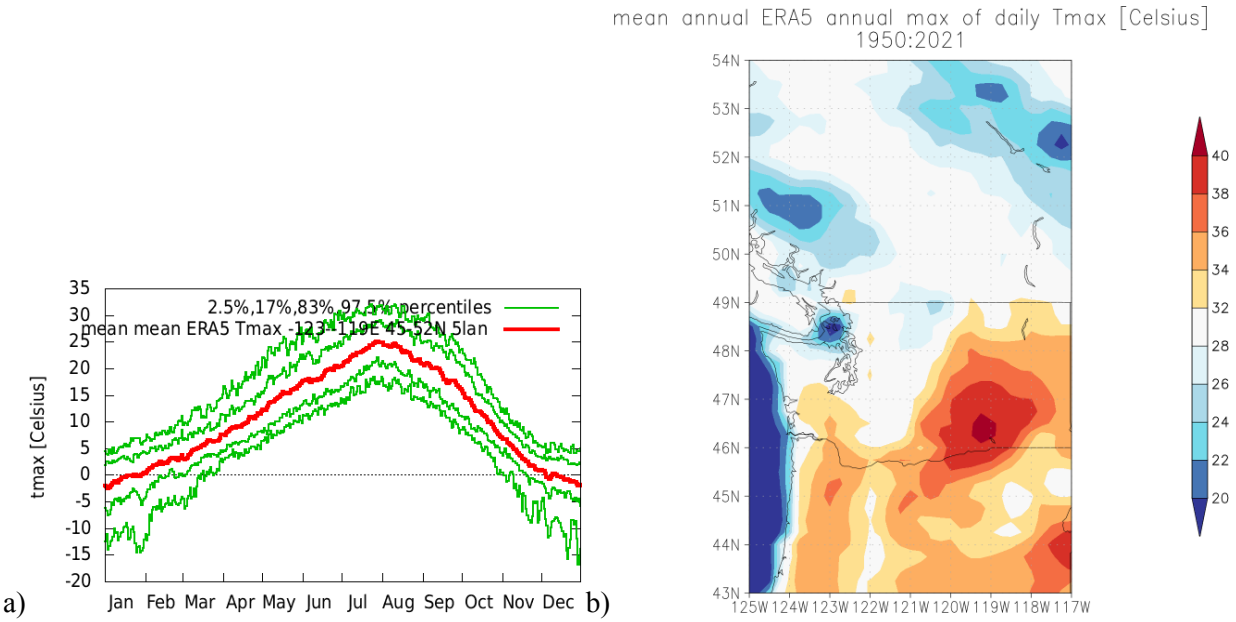

Figure 5. a) Seasonal cycle of Tmax averaged over the land points of 45–52 ºN, 119–123 ºW. b) Spatial pattern of the 1950–2021 mean of the annual maximum of Tmax at each grid point. Based on ERA5.

3.1 Analysis of point station data and gridded data

Figure 6a shows our standard extreme value analysis and the challenge of applying it to this event. The distribution of our index including data up to 2020 is described very well by a GEV distribution that has linearly warmed at a rate about twice as fast as the GMST. This is consistent with the general characteristic of global warming that summers over continents warm faster than the global mean. The fit has a negative shape parameter ξ, which implies a finite tail, and hence an upper bound. In this case it is at 35.5±1.3 ºC (2σ uncertainty). However, the observed value in 2021, 39.5 ºC, is far above this upper bound. Therefore, this GEV fit with constant shape and scale parameters that excludes all information about 2021 is not a valid description of the heatwaves in the area.

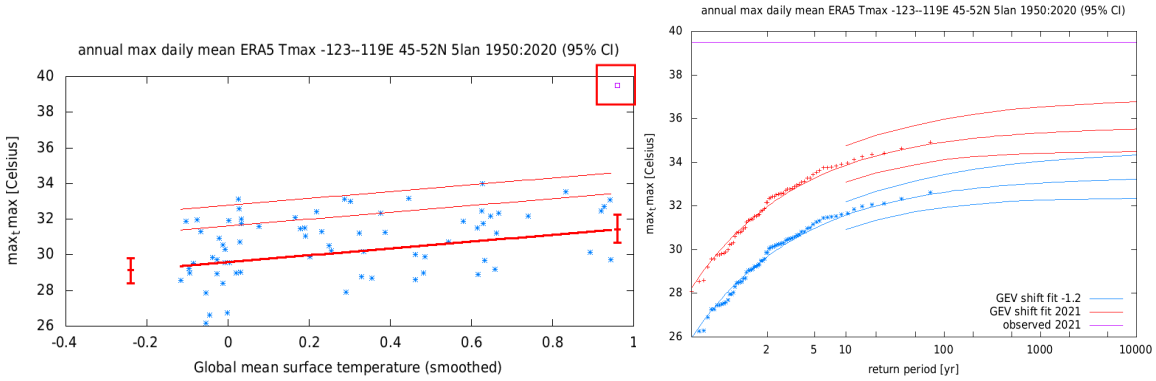

Figure 6. GEV fit with constant scale and shape parameters, and location parameter shifting proportional to GMST of the index series. No information from 2021 is included in the fit. Left: the observed TXx as a function of the smoothed GMST. The thick red line denotes the location parameter, the thin red lines the 6 and 40-yr return times. The June 2021 observation is highlighted with the red box and is not included in this fit. Right: Return time plots for the climate of 2021 (red) and a climate with GMST 1.2 ºC cooler (blue). The past observations are shown twice: once shifted up to the current climate and once shifted down to the climate of the late nineteenth century. Based on ERA5 extended with operational ECMWF analyses for June 2021.

An alternative to the standard approach of not using any information of the event under study to avoid a selection bias, is to use some of the information from the June 2021 heatwave, namely that it actually happened. Specifically, in the next fit we still assume that the data up to 2020 can be described by a GEV with constant scale and shape parameters, but we reject all GEV models in which the upper bound is below the value observed in 2021. In other words, we enforce a distribution that does not a priori reject the 2021 event as impossible. The result is shown in Figure 7. While the distribution now includes the 2021 event, the fit to the data up to and including the year 2020 is noticeably worse than when not taking 2021 into account. This suggests either a low-probability extreme or the contribution of non-linear effects to the event (Section 7). The return time for the 2021 event under these assumptions still has a lower bound of 10,000 years in the current climate. The fit differs from the previous one mainly in the shape parameter, which is now much less negative (about −0.2 instead of −0.4). This shifts the upper bound to higher values. The fit also gives a somewhat higher trend parameter.

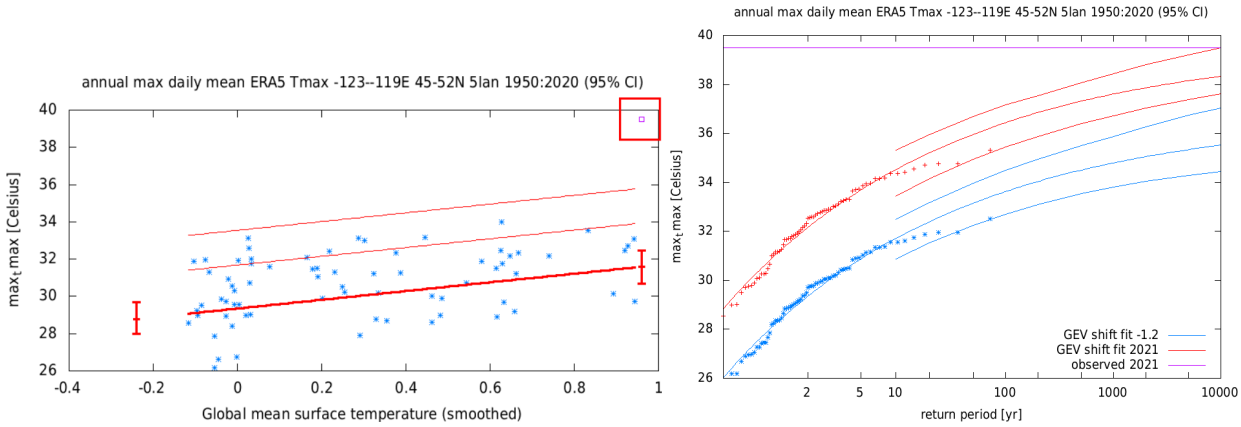

Figure 7. As Figure 6 but demanding the 2021 event is possible in the fitted GEV function, i.e., the upper bound is higher than the value observed in 2021.

The third possibility is to fit the GEV distribution over all available data, including 2021. This yields a return time of 1,000 years (95% CI >100 yr). This approach implicitly assumes that the 2021 event is drawn from the same distribution. This would not be the case if it would be selected from a large pool of time series to have as large a return time as possible. In that case it would be drawn from a larger distribution and could be expected to have a high extreme with a high return period due to selection bias. This is only partly the case here as we did choose the region because the heat was exceptional there. However, we also based our exact choice on population density and type of terrain, parameters that are more independent of the heatwave. The return time of 1000 yr is therefore possibly overestimated. However, this approach uses all information available and assumes this was just a chance event. We use this third approach thus as the best estimate, although follow-up research will be necessary to assess if possible non-linear effects could be consistent with the behaviour found with the other two fits (see also Section 7).
This fit gives a 95% CI of 1.4 to 1.9 K for the scale parameter σ and -0.5 to 0.0 for the shape parameter ξ. These values are used in section 4, the model validation.

The detection results, i.e., the comparison of the fit for 2021 and for a pre-industrial climate, show an increase in intensity of TXx of $\Delta T = 3.1$ ºC (95% CI: 1.1 to 4.7 ºC) and a probability ratio PR of 350 (3.2 to ∞).

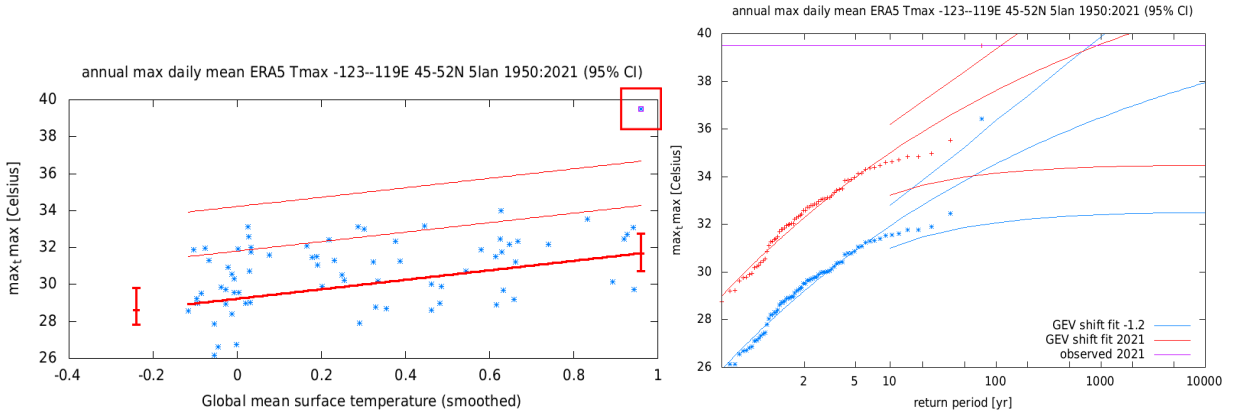

Figure 8. As for Figure 6 but including data from the 2021 heatwave into the fit.

We can give a very rough estimate of the global return time of a sudden jump in TXx with a similar return time. Assuming it was just a chance event, the heatwave covers an area of O(1500 km)², which is about 1.5% of the land area of the world. From this we can estimate the return time of a similar heatwave in terms of low probability and area covered, as there are about 1/(1.5%) ~ 60 independent areas in which it could have occurred. This implies that the return time of an event as rare as this one or rarer, somewhere over land, is 60 times larger than the O(1000 yr) that it occurred at the specific location that it did. This gives a very rough estimate of O(15 yr) with a lower bound of O(1.5 yr) to have such an improbable heatwave somewhere on the land of the earth. It is therefore conceivable that it was pure chance that it happened at this location. Further research on this and other exceptional heatwaves will be needed to determine whether this estimate is indeed realistic.

3.2 Analysis of temperature in Portland, Seattle and Vancouver

For Portland we choose the International Airport station, which is located on the northern edge of the city and has data starting in April 1938 and continuing until yesterday in the GHCN-D v2 database. Figure 9 (top panel) shows the annual maxima of the Portland station time series, assuming there will be no higher value during the rest of the summer. The record before this year was 41.7 ºC in 1965 and 1981, and TXx reached 46.7 °C this year, so the previous record was broken by 5.0 ºC.

We fit a GEV distribution to this data, including 2021 (Figure 9, lower panels). It gives a return time of 700 yr with a lower bound of 70 yr. For the PR we can only give a lower bound of 6, the best estimate is infinite. This corresponds to an increase in temperature of 3.4 ºC with a large uncertainty of 0.3 to 5.3 ºC. The large uncertainties are due to the somewhat shorter time series and large variability at this station.

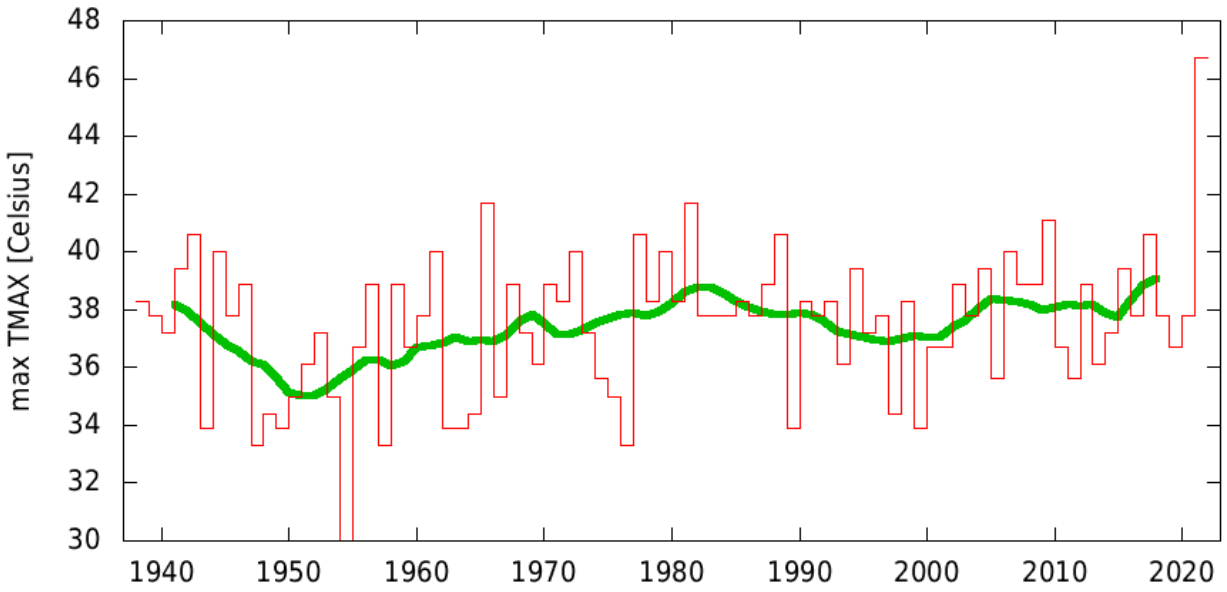

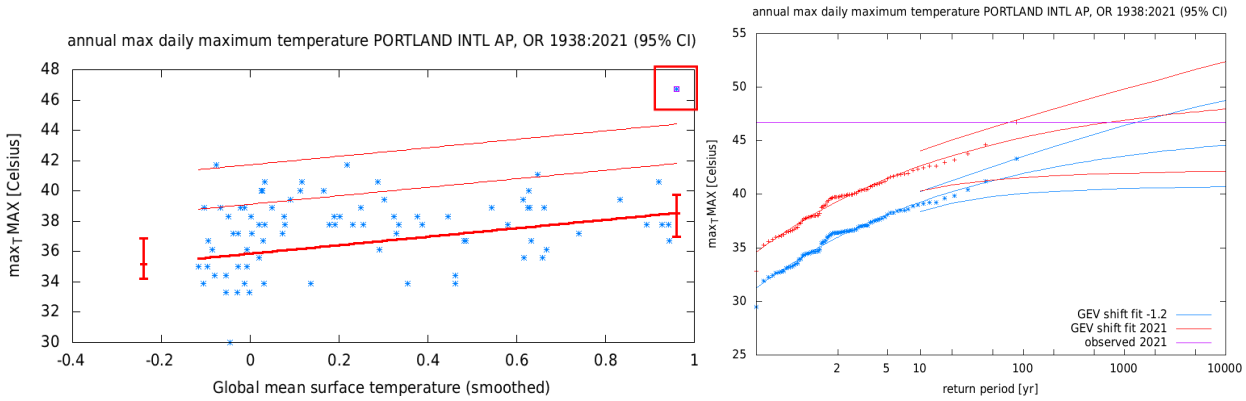

Figure 9: Top: time series of observed highest daily maximum temperature of the year at Portland International Airport. Bottom: as Figure 8 but for the station data at Portland International Airport. Source: data GHCN-D, fit: KNMI Climate Explorer.

In Seattle, the only station with a sufficiently long time series that includes 2021 is Seattle-Tacoma International Airport. It is located ~15 km south of the city but has similar terrain, without the upstream lakes of the city itself. The previous record was 39.4 ºC in 2009, and this year it reached 42.2 ºC. This is still a large increase of 2.8 ºC over the previous record. The event was also not quite as improbable, with a return time of 300 yr (lower bound 40 yr) in the current climate (Figure 10). The PR is again infinite with a lower bound of 7, and the increase in temperature from a late nineteen century climate is 3.8 ºC (0.7 to 5.7 ºC).

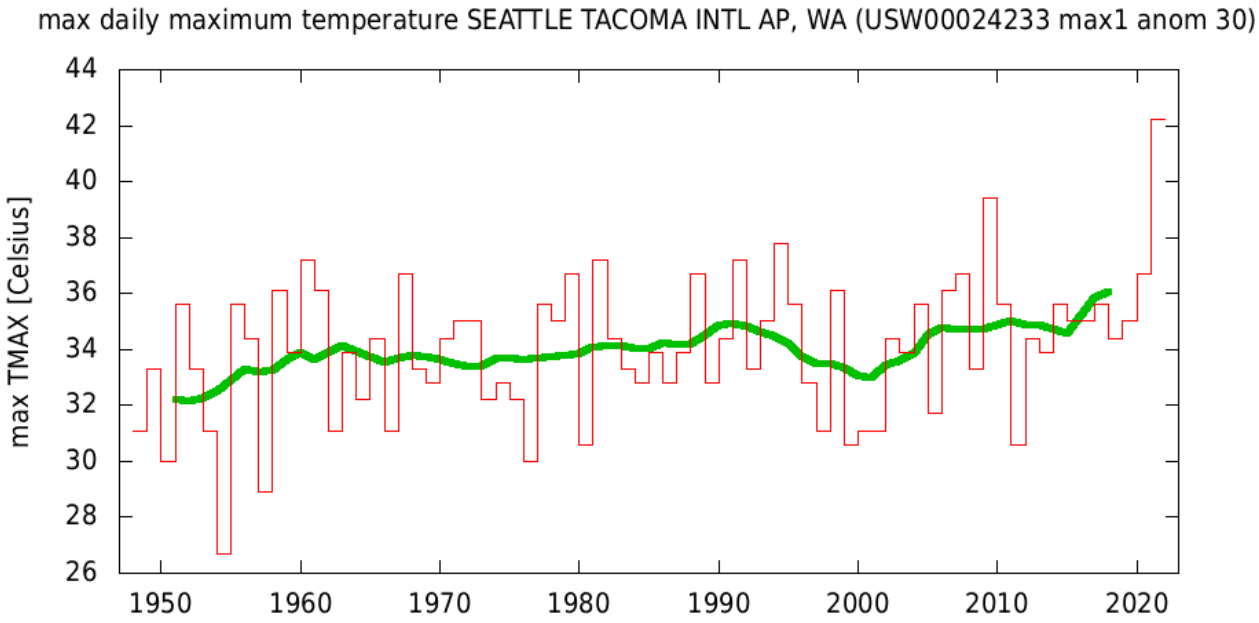

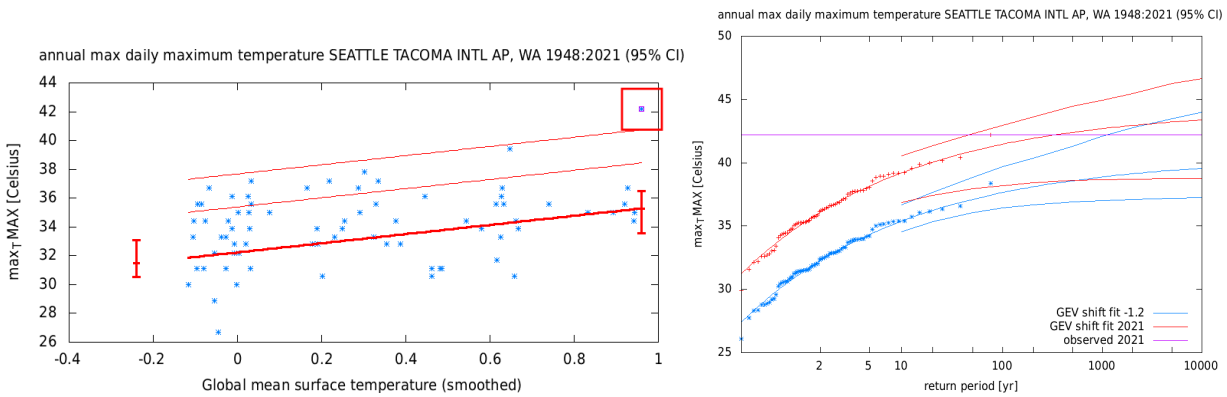

Figure 10: as Figure 9 but for the station data at Seattle-Tacoma International Airport. Source: data GHCN-D, fit: KNMI Climate Explorer.

In the Vancouver area the most representative station with fewest missing data is New Westminster. It has data from 1875 to 2021 with a few gaps. The previous record was 37.6 ºC in 2009, and in 2021 a temperature of 41.4 ºC was observed, 4.0 ºC warmer. A GEV fit including 2021 gives a return time of 1000 yrs with a lower bound of 70 yr (Figure 11). The PR is infinite with a lower bound of 170, and the temperature has increased by 3.4 (1.9 to 5.5) ºC.

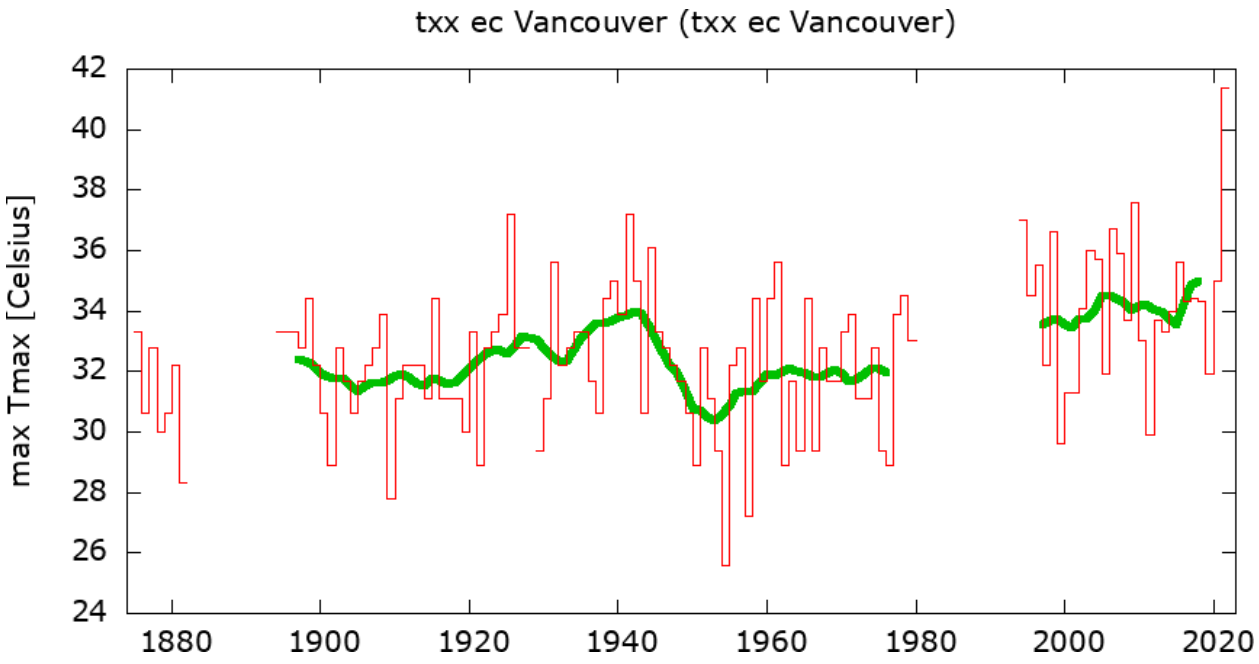

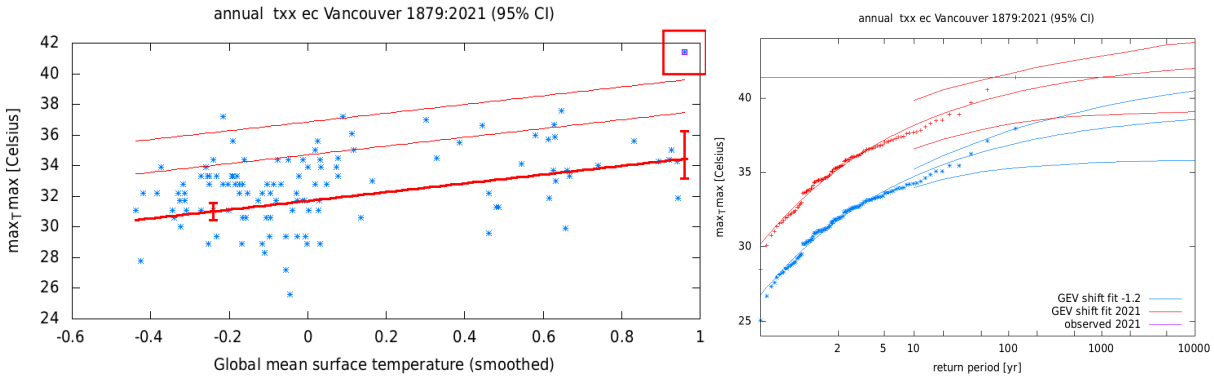

Figure 11: as Figure 9 but for the station data at New Westminster. Source: data EC, fit: KNMI Climate Explorer.

4 Model evaluation

In this section we show the results of the model validation. The validation criteria assess the similarity between the modelled and observed seasonal cycle, the spatial pattern of the climatology, and the scale and shape parameters of the GEV distribution. The assessment results in a label "good", "reasonable" or "bad", according to the criteria defined in Philip et al. 2020. In this study, we use models that are labelled "good" or "reasonable". However, if five or more models classify as "good" within a particular framing such as the CMIP6 models, then we do not include all of the "reasonable" models but only those that pass the test on fit parameters as "good". Table 1 shows the model validation results. The full table including also the models that did not pass the validation tests is given in Table 3. 21 models and a combined 224 ensemble members passed the validation test.

Table 1. Validation results for models that pass the validation tests on seasonal cycle, spatial pattern and GEV scale and shape fit parameters sigma. Observations in blue, models in black.

Model / Observations	**Seasonal cycle**	**Spatial pattern**	**Sigma**	**Shape parameter**	**Conclusion**
ERA5			1.70 (1.40 ... 1.90)	-0.200 (-0.500 ... 0.00)	
GFDL-CM2.5/FLOR historical-rcp45 (5)	good	good	2.01 (1.84 ... 2.17)	-0.201 (-0.272 ... -0.144)	reasonable, include as different experiment than most other models
ACCESS-CM2 historical-ssp585 (2)	good	good	1.86 (1.71 ... 2.02)	-0.200 (-0.260 ... -0.120)	good
AWI-CM-1-1-MR historical-ssp585 (1)	good	good	1.50 (1.35 ... 1.69)	-0.200 (-0.280 ... -0.110)	good
CNRM-CM6-1 historical-ssp585 (1)	good	good	1.54 (1.39 ... 1.72)	-0.210 (-0.290 ... -0.100)	good
CNRM-CM6-1-HR historical-ssp585 (1)	good	good	1.48 (1.33 ... 1.66)	-0.190 (-0.270 ... -0.100)	good

CNRM-ESM2-1 historical-ssp585 (1)	good	good	1.71 (1.54 ... 1.92)	-0.180 (-0.250 ... -0.0900)	good
CanESM5 historical-ssp585 (50)	good	reasonable	1.79 (1.76 ... 1.82)	-0.180 (-0.190 ... -0.170)	reasonable, include because statistical parameters good
EC-Earth3 historical-ssp585 (3)	good	good	1.87 (1.76 ... 2.00)	-0.220 (-0.270 ... -0.170)	good
FGOALS-g3 historical-ssp585 (3)	good	reasonable	1.80 (1.69 ... 1.92)	-0.180 (-0.210 ... -0.140)	reasonable, include because statistical parameters good
GFDL-CM4 historical-ssp585 (1)	good	good	1.43 (1.29 ... 1.62)	-0.210 (-0.300 ... -0.110)	good
INM-CM4-8 historical-ssp585 (1)	good	good	1.63 (1.46 ... 1.83)	-0.210 (-0.300 ... -0.110)	good
INM-CM5-0 historical-ssp585 (1)	good	good	1.80 (1.63 ... 2.03)	-0.240 (-0.310 ... -0.140)	good
IPSL-CM6A-LR historical-ssp585 (6)	good	reasonable	1.79 (1.71 ... 1.88)	-0.220 (-0.250 ... -0.180)	reasonable, include because statistical parameters good
MIROC-ES2L historical-ssp585 (1)	reasonable, peaks about a month early	reasonable	1.46 (1.31 ... 1.65)	-0.190 (-0.300 ... -0.0900)	reasonable, include because statistical parameters good
MPI-ESM1-2-HR historical-ssp585 (2)	good	good	1.49 (1.39 ... 1.62)	-0.250 (-0.310 ... -0.190)	good
MPI-ESM1-2-LR historical-ssp585 (10)	good	good	1.63 (1.58 ... 1.69)	-0.260 (-0.280 ... -0.230)	good
MRI-ESM2-0 historical-ssp585 (2)	reasonable, peak too flat	good	1.41 (1.30 ... 1.53)	-0.280 (-0.340 ... -0.220)	reasonable, include because statistical parameters good
NESM3 historical-ssp585 (1)	good	good	1.48 (1.34 ... 1.67)	-0.290 (-0.370 ... -0.200)	good
NorESM2-MM historical-ssp585 (1)	good	good	1.90 (1.70 ... 2.12)	-0.250 (-0.350 ... -0.140)	in between reasonable and good, include
IPSL-CM6A-LR historical-ssp245 (32)	good, from CMIP6	reasonable, from CMIP6	1.69 (1.64 ... 1.75)	-0.220 (-0.250 ... -0.200)	reasonable, obs covar used, different from CMIP6 as different ssp scenario. Use both
CAM5-1-1degree C20C historical (99)	NA	NA	1.70 (1.68 ... 1.72)	-0.176 (-0.172 ... -0.180)	good, values used with warming level 1.7

5 Multi-method multi-model attribution

This section shows probability ratios and change in intensity ΔT for models that pass the validation tests and also includes the values calculated from the fits to observations (Table 2). Results are given both for

changes in current climate (1.2°C) compared to the past (pre-industrial conditions) and, when available, for a climate at +2˚C of global warming above pre-industrial climate compared with current climate. The results are visualized in Section 6.

Table 2. Analysis results showing the model threshold for a 1-in-1000 year event in the current climate, and the probability ratios and intensity changes for the present climate with respect to the past (labelled "past") and for the +2C GMST future climate with respect to the present (labelled "future").

Model / Observations	**Threshold**	**Probability ratio PR - past [-]**	**Change in intensity ΔT - past [˚C]**	**Probability ratio PR - future [-]**	**Change in intensity ΔT - future [˚C]**
ERA5	39.5 ˚C	3.5e+2 (3.2 ... ∞)	3.1 (1.1 ... 4.7)		
GFDL-CM2.5/FLOR historical-rcp45 (5)	34 ˚C	6.5e+2 (16 ... ∞)	1.6 (1.2 ... 2.1)	4.6 (3.4 ... 12)	1.2 (1.0 ... 1.3)
ACCESS-CM2 historical-ssp585 (2)	35 ˚C	25 (2.3 ... ∞)	1.1 (0.41 ... 1.9)	45 (4.5 ... ∞)	1.2 (0.96 ... 1.4)
AWI-CM-1-1-MR historical-ssp585 (1)	36 ˚C	1.1e+4 (6.6 ... ∞)	1.6 (0.84 ... 2.3)	2.8e+2 (5.5 ... ∞)	1.3 (1.1 ... 1.6)
CNRM-CM6-1 historical-ssp585 (1)	34 ˚C	1.9 (0.0 ... ∞)	0.22 (-0.51 ... 0.95)	69 (3.4 ... ∞)	1.1 (0.76 ... 1.3)
CNRM-CM6-1-HR historical-ssp585 (1)	35 ˚C	5.2e+2 (5.4 ... ∞)	1.5 (0.73 ... 2.2)	56 (4.1 ... ∞)	1.3 (1.0 ... 1.5)
CNRM-ESM2-1 historical-ssp585 (1)	38 ˚C	1.5e+2 (3.6 ... ∞)	1.6 (0.68 ... 2.6)	15 (2.8 ... ∞)	0.97 (0.64 ... 1.3)
CanESM5 historical-ssp585 (50)	38 ˚C	1.6e+3 (2.6e+2 ... 6.7e+4)	2.0 (1.9 ... 2.1)	62 (32 ... 1.5e+2)	1.5 (1.4 ... 1.5)
EC-Earth3 historical-ssp585 (3)	38 ˚C	3.2e+2 (8.2 ... ∞)	1.3 (0.88 ... 1.7)	20 (5.2 ... 5.8e+2)	1.2 (1.1 ... 1.4)
FGOALS-g3 historical-ssp585 (3)	41 ˚C	71 (8.5 ... 2.1e+8)	1.5 (1.0 ... 2.0)	17 (5.2 ... 2.2e+2)	1.1 (0.87 ... 1.3)
GFDL-CM4 historical-ssp585 (1)	31 ˚C	∞ (14 ... ∞)	2.1 (1.3 ... 3.0)	∞ (16 ... ∞)	1.7 (1.4 ... 1.9)
INM-CM4-8 historical-ssp585 (1)	42 ˚C	∞ (28 ... ∞)	2.6 (1.7 ... 3.6)	2.7e+3 (6.5 ... ∞)	1.7 (1.4 ... 2.0)
INM-CM5-0 historical-ssp585 (1)	41 ˚C	∞ (14 ... ∞)	2.2 (0.95 ... 3.3)	∞ (12 ... ∞)	1.6 (1.3 ... 2.0)
IPSL-CM6A-LR historical-ssp585 (6)	34 ˚C	1.5e+5 (50 ... ∞)	1.7 (1.4 ... 2.0)	2.4e+2 (16 ... ∞)	1.3 (1.1 ... 1.4)
MIROC-ES2L historical-ssp585 (1)	33 ˚C	75 (1.3 ... ∞)	1.2 (0.040 ... 2.3)	12 (2.2 ... ∞)	0.71 (0.41 ... 1.0)
MPI-ESM1-2-HR historical-ssp585 (2)	34 ˚C	∞ (27 ... ∞)	1.4 (0.82 ... 1.9)	4.8e+4 (12 ... ∞)	1.2 (0.96 ... 1.4)

MPI-ESM1-2-LR historical-ssp585 (10)	32 ˚C	∞ (1.1e+11 ... ∞)	1.6 (1.4 ... 1.9)	∞ (1.8e+3 ... ∞)	1.3 (1.2 ... 1.4)
MRI-ESM2-0 historical-ssp585 (2)	32 ˚C	∞ (1.3e+2 ... ∞)	1.4 (0.86 ... 1.9)	13 (4.9 ... 54)	1.0 (0.84 ... 1.2)
NESM3 historical-ssp585 (1)	30 ˚C	∞ (1.1e+5 ... ∞)	2.5 (1.9 ... 3.2)	∞ (66 ... ∞)	1.5 (1.3 ... 1.7)
NorESM2-MM historical-ssp585 (1)	41 ˚C	∞ (11 ... ∞)	2.6 (1.3 ... 3.9)	4.3e+7 (7.0 ... ∞)	1.7 (1.3 ... 2.1)
IPSL-CM6A-LR historical-ssp585 (32)	34 ˚C	∞ (∞ ... ∞)	2.6 (2.4 ... 2.9)	-	-
CAM5-1-1degree C20C historical ()	43 ˚C	2.4e+2 (1.5e+2 ... 3.8e+2)	1.6 (1.5 ... 1.8)	-	-

6 Hazard synthesis

We calculate the probability ratio as well as the change in magnitude of the event in the observations and the models. We synthesise the models with the observations to give an overarching attribution statement (please see e.g. Kew et al. (2021) for details on the synthesis technique including how weighting is calculated for observations and for models). Observations and models are combined into a single result in two ways. Firstly, we neglect common model uncertainties beyond the averaged model spread that is depicted by the bright red bar, and compute the weighted average of models and observations: this is indicated by the magenta bar. The weighting applied is the inverse square of the variability (the width of the bright bars). As, due to common model uncertainties, model uncertainty can be larger than the model spread, secondly, we also show the more conservative estimate of an unweighted average of observations and models, indicated by the white box accompanying the magenta bar in the synthesis figures.

Figure 12 shows the synthesis results for the current vs. past climate; the results for the future vs. current climate are presented in Figure 13. Where the results for the probability ratio do not give a finite number we replace them by 10000, to allow all models to be included in the synthesis analysis. This means that the reported synthesized probability ratio gives a more conservative, lower value. For the intensity change we report the weighted synthesis value. For probability ratio we can only give a lower estimate of the range.

Results for current vs past climate, i.e. for 1.2°C of global warming vs pre-industrial conditions (1850-1900), indicate an increase in intensity of about 2.0 ˚C (1.2 ˚C to 2.8 ˚C) and a PR of at least 150. Model results for additional future changes if global warming reaches 2°C indicate another increase in intensity of about 1.3 ˚C (0.8 ˚C to 1.7 ˚C) and a PR of at least 3, with a best estimate of 175. This means that an event like the current one, that is currently estimated to occur only once every 1000 years, would occur roughly every 5 to 10 years in that future world with 2°C of global warming.

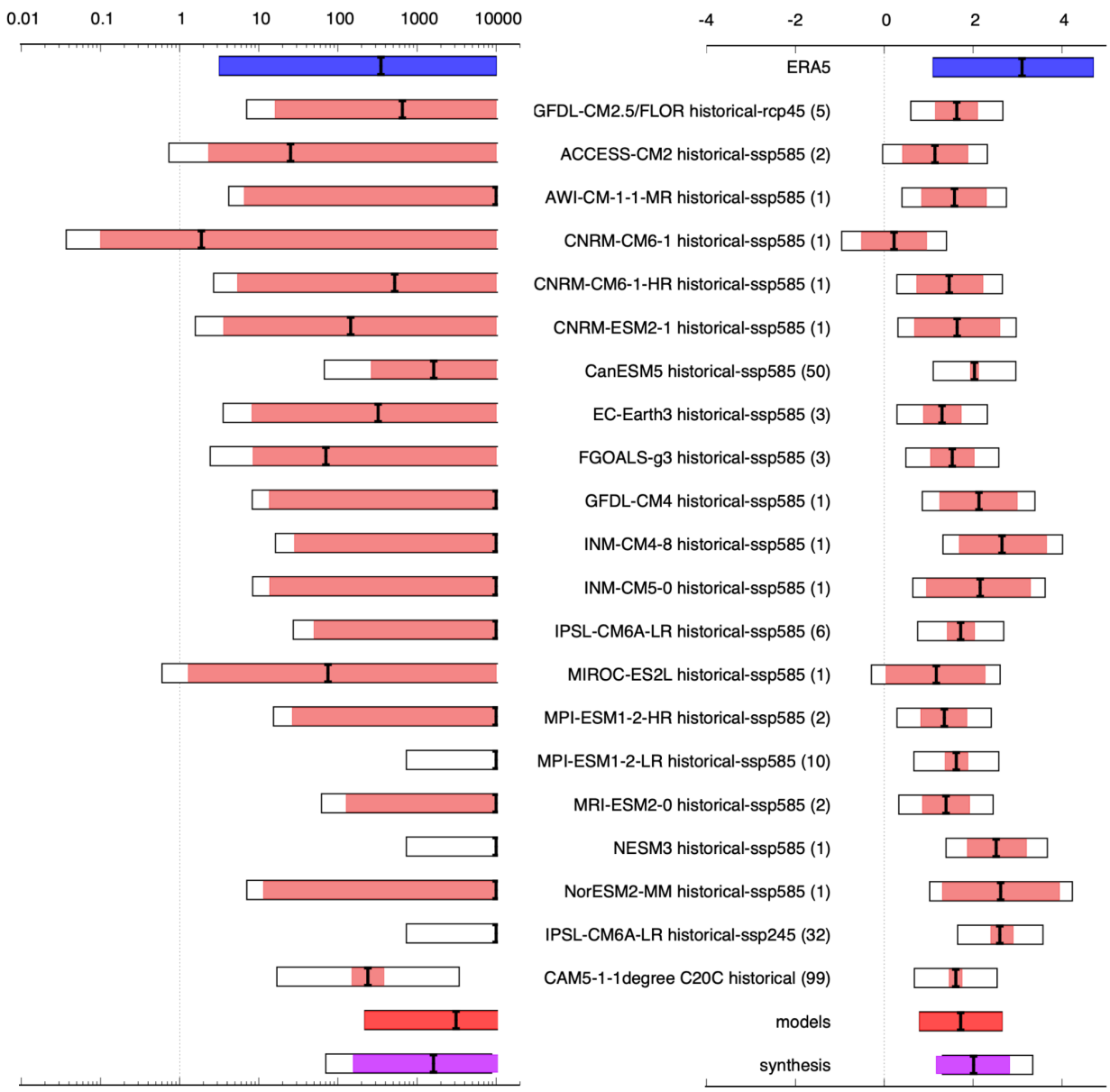

Figure 12. Synthesis of the past climate, showing probability ratios (left) and changes in intensity in ˚C (right), comparing the 2021 event with a pre-industrial climate.

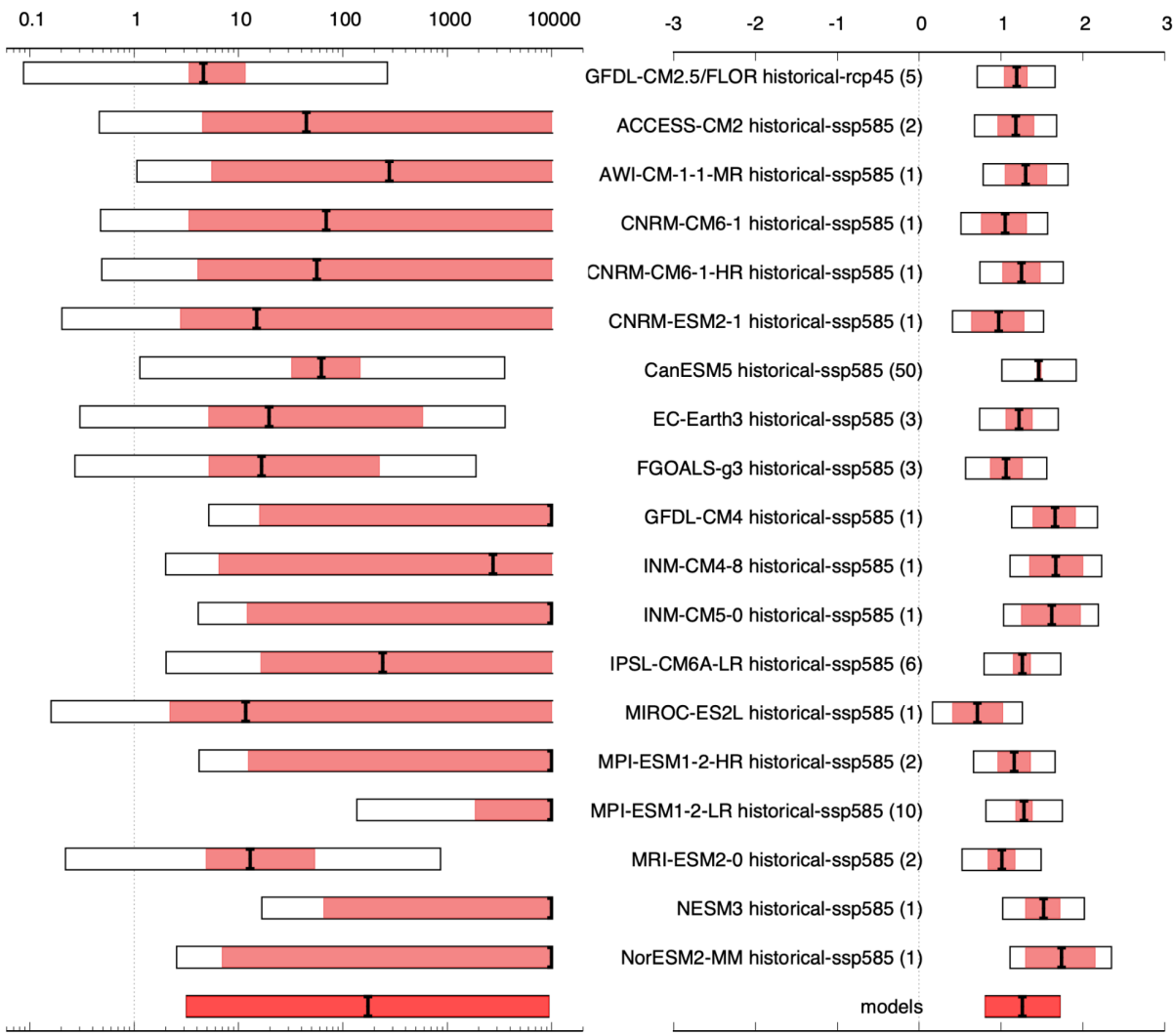

Figure 13. Same as Figure 12 but comparing 2°C of global warming (above pre-industrial) with present-day values.

7 Meteorological conditions and drivers

7.1 Meteorological analysis and dynamics

The evolution of this event can be explained by a confluence of meso- and synoptic-scale dynamical features, potentially including antecedent low-moisture conditions. At the synoptic scale, an omega-block developed over the study area beginning at roughly 00UTC on June 25th centred at ~125 ˚W, 52 ˚N, which then very slowly progressed eastward over subsequent days. This ridge featured a maximal 500 hpa geopotential height of ~5980 m, which is unprecedented for this area of western North America for the period from 1948 through to June 2021 at least (Figure 14).

Despite being a record, this extreme high pressure system – sometimes called a "Heat dome" – is not that anomalous given the long-term trend in 500 hPa driven by thermal expansion (Christidis and Stott, 2015). Also, comparing recent heatwaves in the Pacific NW to the extreme heatwave in Western Europe in 2019 (Vautard et al., 2020), the geopotential height reached similar anomalies and has a similar long-term trend (Figure 14).

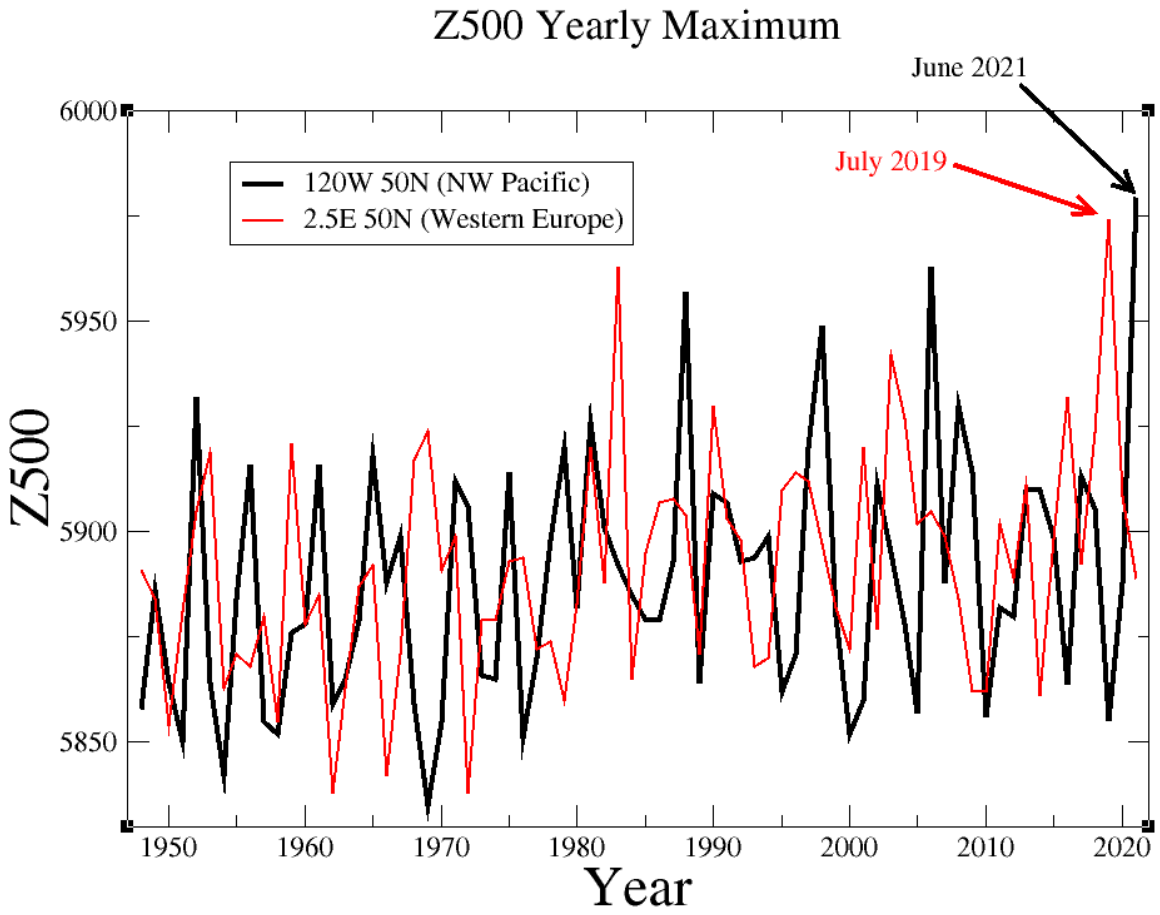

Figure 14: 500 hPa height (m) yearly maximum for two points at same latitude in two continents. Black: Pacific NW (as above) and red: Western Europe (2.5E; 50N).

The circulation pattern itself also appears not extremely anomalous: using analogues of 500 hPa and a pattern correlation metric to compare fields, we find that about 1% of June and July circulation patterns, defined as the 500 hPa geopotential height pattern within [160 ˚W-110 ˚W ; 35 ˚N-65 ˚N] in previous years have an anomaly correlation larger than 0.8 with the 28 June pattern. This degree of correlation is typical among days with this type of blocking pattern during the months of June and July., Roughly one third of June and July geopotential height fields have 1% or fewer analogues with an anomaly correlation larger than 0.8. We also find that this fraction does not change when restricting the analogues search within 3 distinct time periods between 1948 and 2020. We conclude that the 28 June circulation is likely not exceptional, while temperatures associated with it were.

At the meso-scale, high solar irradiance during the longest days of the year and strong subsidence increased near-surface air temperatures during the event. As is typical for summer heatwaves in the region

(Brewer et al., 2012; Brewer et al., 2013), a meso-scale thermal trough developed and reached southwest Oregon by 00UTC on the 28th June. This feature migrated northward reaching the northern tip of Washington State by 00UTC on the 29th. Further offshore, a small cut-off low travelled southwest to northeast around the synoptic-scale trough that made up the west arm of the omega block. The pressure gradients associated with the thermal trough and the cut-off low promoted moderate E-SE flow in the northern and eastern sectors of the feature and S-SW flow to the south. Near-surface winds with easterly components crossed the Cascade Range of Washington and Oregon and the southern Coast Mountains of British Columbia. The difference in elevation on the west and east sides of the mountain ranges contributed to more adiabatic heating than cooling, which helped drive the warmest temperatures observed in the event along the foot of the west slope of these mountains, at sea level. These dynamics are illustrated in Figure 15. By 12UTC on the 29th of June 2021, all but the eastern edge of the study area was under the influence of southerly to southwesterly near surface flows that advected marine air and forced marked cooling.

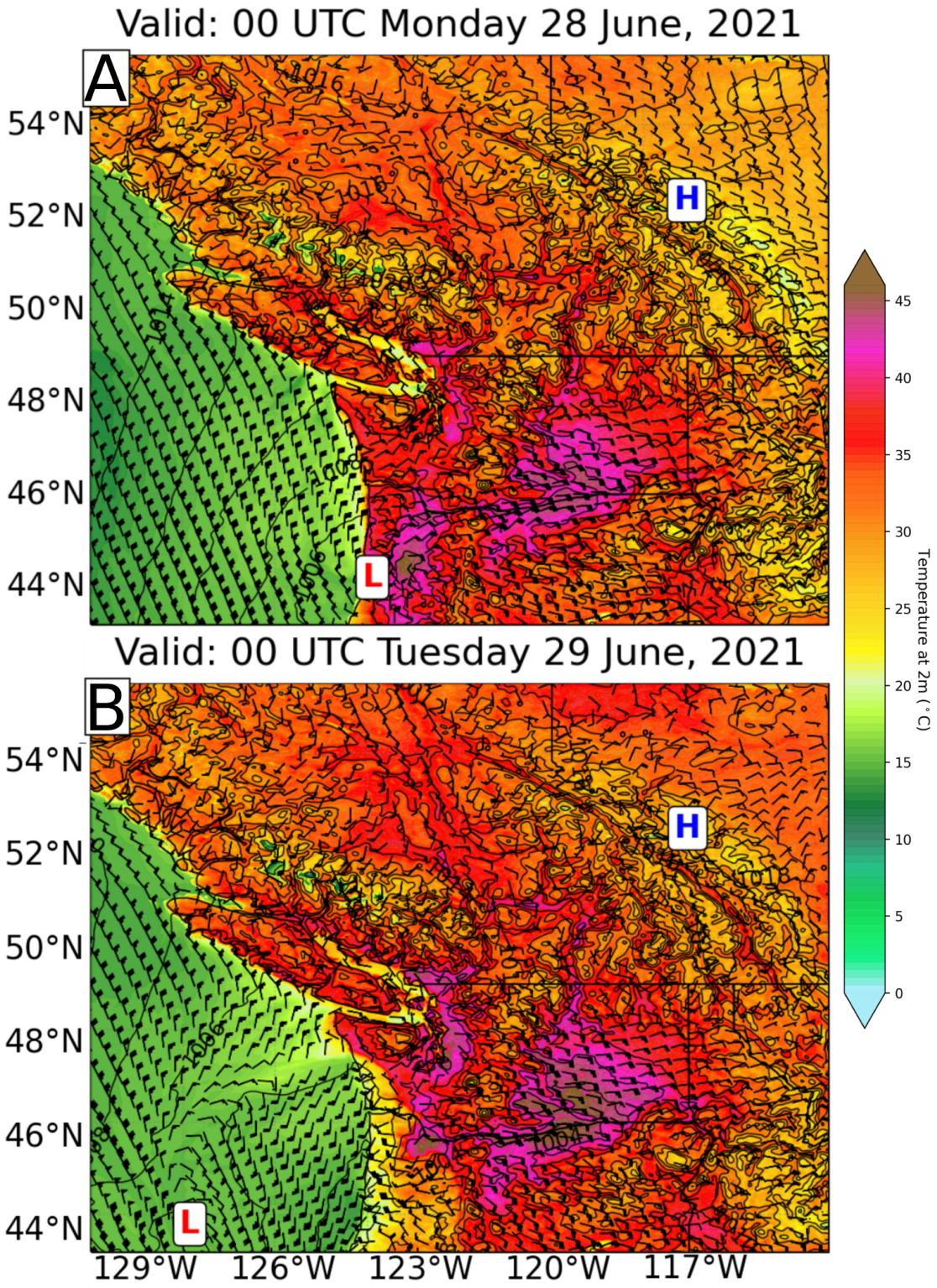

Figure 15. Regional simulation of sea level pressure, 2m air temperature, and 10m wind velocity in the region containing the study area using the Weather Research and Forecasting (WRF; Skamarock et al., 2019) model forced by the North American Mesoscale Forecast System (NAM). Panel (A) shows the situation during the peak of the event for the part of the study area south of Portland at 5PM local time.

Panel (B) as in (A) but for 5PM local time on the day of peak temperature for Portland, Seattle and Vancouver.

There is no scientific consensus whether blocking events are made more severe or persistent because of Arctic amplification or other mechanisms (i.e. Tang et al, 2014; Barnes and Screen, 2015; Vavrus, 2018).We contend that Arctic sea-ice was unlikely to have played a large role in this event largely due to the timing. In early summer, Arctic sea ice remains extensive, but is melting thus keeping near surface temperatures near 0 ºC. This causes summer trends in near-surface temperatures over the Arctic ocean to be lower than the midlatitudes. During recent months, the sea ice extent was below the 1981-2010 mean, but was similar to values observed from 2011 to 2020 (Fetterer et al., 2017). Instead, Arctic Amplification in summer is characterized by strong warming over high-latitude land areas (as can clearly be seen in Figure 16) and this warming signal reaches into the upper-troposphere. This enhanced warming is likely related to strong downward trends in early summer snow cover. There is evidence, from observations (Coumou et al, 2015; Chang et al, 2016), climate models (Harvey et al, 2020; Lehmann et al, 2014) and paleo-proxies (Routson et al, 2019), that this enhanced warming over high latitudes leads to a weakening of the jet and storm tracks in summer. This weakening could favour more persistent weather conditions (Pfleiderer et al, 2019; Kornhuber & Tamarin-Brodsky, 2021). Regional-scale interactions between loss of snow cover and low soil moisture associated with earlier snowmelt and rapid springtime soil moisture drying, may have had an enhanced warming impact into early summer in the Arctic. At mid-atmospheric levels there is some amplification remaining due to the winter season (Figure 16), but at the jet level (~250 hPa) the usual increase of the thermal gradient due to tropical upper tropospheric warming is advected North by the Hadley circulation (Haarsma et al, 2013). The final effect on the jet stream is therefore a competition between factors enhancing and decreasing the temperature gradient.

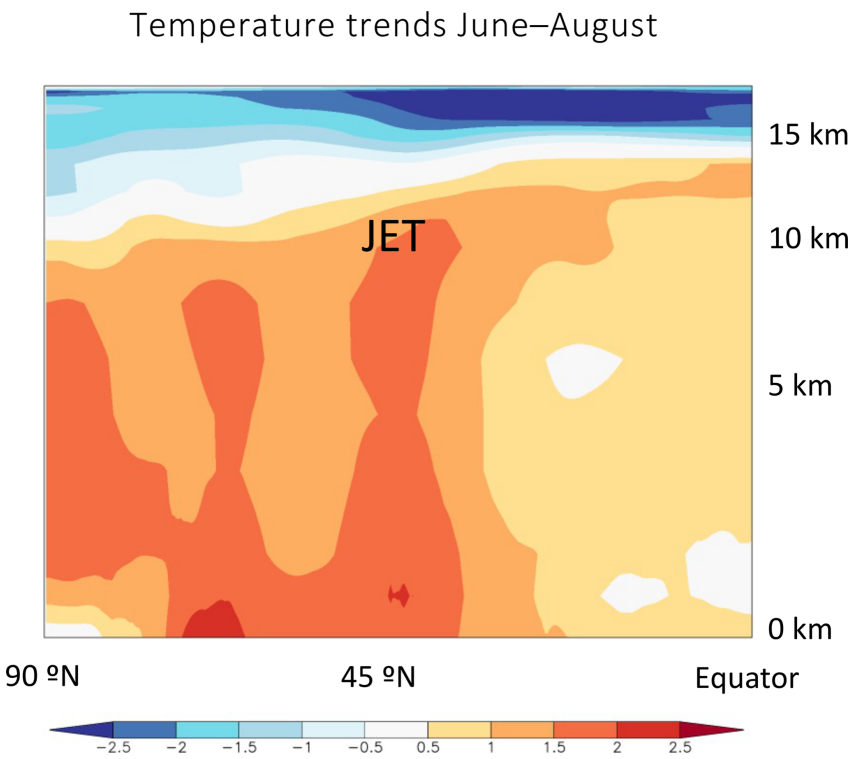

Figure 16. Zonal mean trends in temperature (ºC per degree global warming) as function of pressure in the ERA5 reanalysis 1979–2019 in the northern hemisphere.

7.2 Drought

An additional feature of the event is the very dry antecedent conditions that may have contributed to observed extreme temperatures through reduced latent cooling from low evapotranspiration rates. Low soil moisture conditions can lead to a strong amplification of temperature during heatwaves, including non-linear effects (Seneviratne et al. 2010, Mueller and Seneviratne 2012, Hauser et al. 2016, Wehrli et al. 2019). In addition, low spring snow level conditions can also further amplify this feedback (Hall et al. 2008). Integrated Multi-satellitE Retrievals for the Global Precipitation Mission (IMERG) estimates of precipitation during the period from March through June, 2021 indicate anomalously dry conditions from southern BC southward through California (Figure 17). The precipitation anomaly ranges from close to zero over the Puget Sound area including Seattle to values of between −0.6 and −0.8, meaning that only 20-40% of the average amount of precipitation fell in these locations, in Western Oregon. Note that in the northern parts of the area affected by the heatwave, i.e. in the coastal mountains north of Vancouver Island, large positive precipitation anomalies occurred over recent months.

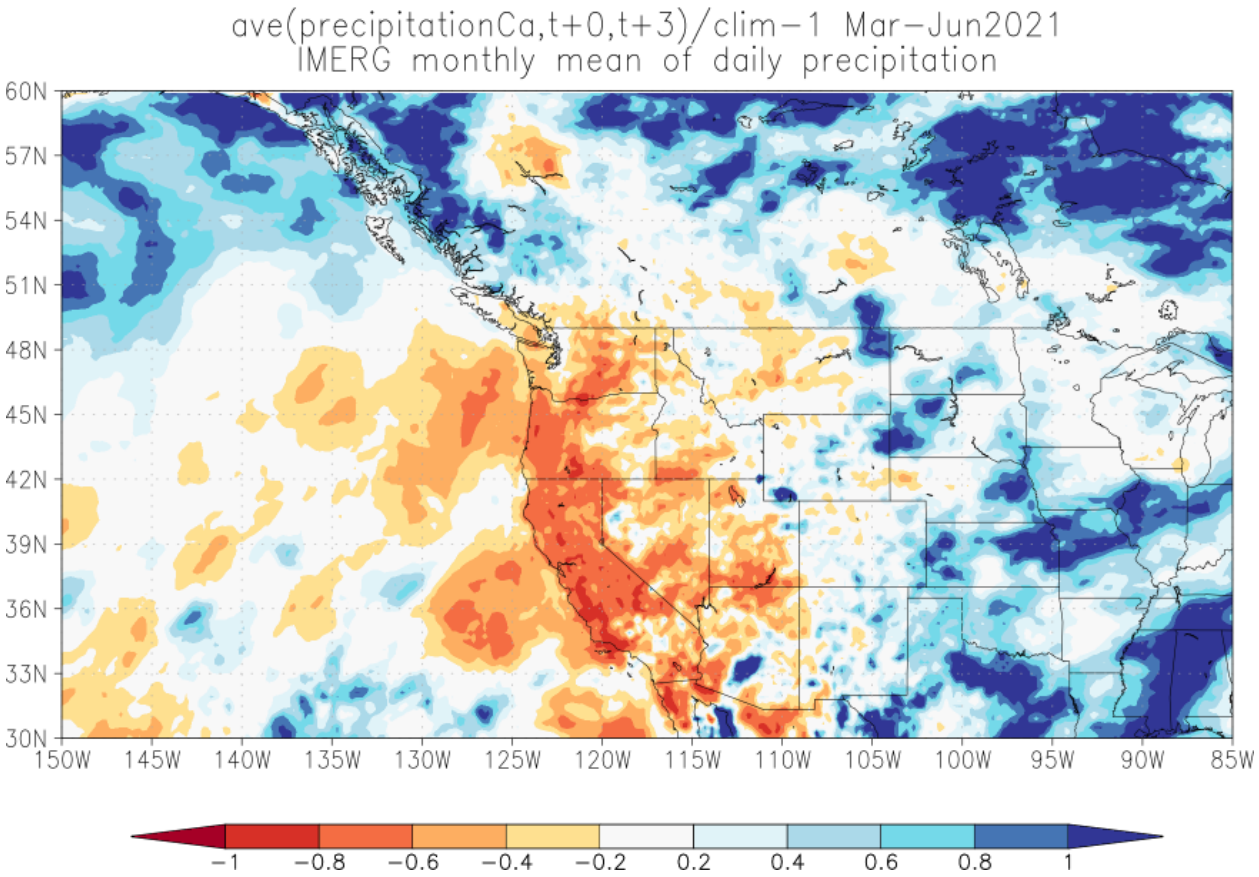

Figure 17. GPM/IMERG satellite estimates of relative precipitation anomalies in March–June 2021 relative to the whole record (2000-2020). The value –1 (dark red) denotes no precipitation, –0.5 (orange) 50% less than normal and zero (light grey) normal precipitation.

The available moisture is also influenced by evapotranspiration, which depends strongly on temperature, radiation and available atmospheric moisture. Evaporation was close to normal in the ERA5 reanalysis March–May in this area (not shown), so does not seem to have played a large role in setting the stage for the heatwave.

Satellite-based measurements of surface soil moisture based on microwave remote sensing from the European Space Agency (ESA) Climate Change Initiative (CCI) provided by the Copernicus service suggest that surface soil moisture was below normal in the region since the beginning of April and that the anomalous conditions persisted until June (https://dataviewer.geo.tuwien.ac.at/?state=88bf0c), in agreement with the decreased precipitation and close to normal evapotranspiration in the ERA5 reanalysis.

7.3 Influence of modes of natural variability

The El Niño Southern Oscillation is the dominant source of interannual variability in the region through the Pacific North American teleconnection. The influence is typically greatest in late winter and spring

and has less clear impacts during summer and fall. Because ENSO was neutral during the preceding months and the impacts on TXx are minimal (r<0.1) we conclude that it had no influence on the occurrence of the heatwave.

The Pacific Decadal Oscillation (PDO) can affect some aspects of North American summer weather, although again the connections to heatwaves in this region are very weak. The strongly negative values of the PDO index, as they occurred in May, would slightly favor cooler conditions for this region. PDO thus also is unlikely to have played an important role in the event.

Altogether, external modes of variability appear to have played little to no role in the formation of the event.

8 Vulnerability and exposure

The Pacific Northwest region is not accustomed to very hot temperatures such as those observed during the June 2021 heatwave. Heatwaves are one of the deadliest natural hazards, resulting in high excess mortality through direct impacts of heat (e.g. heat stroke) and by exacerbating pre-existing medical conditions linked to respiratory and cardiovascular issues (Haines et al., 2006). News reports indicate that there was an increase in emergency calls, emergency department visits, and deaths linked to the heatwave.[7][8] In the following weeks and months, official data on excess deaths will become available to quantify the full extent of the human impacts on human health. The June 2021 heatwave also affected critical infrastructure such as roads and rail and caused power outages, agricultural impacts, and forced many businesses and schools to close[9] [10]. Rapid snowmelt in BC caused water levels to rise, also leading to evacuation orders north of Vancouver.[11] Furthermore, in some places, wildfires, the risk of which has increased due to climate change in this region (Kirchmeier-Young et al., 2018), have started and quickly spread requiring entire towns to evacuate[12]. The co-occurence of such events may result in compound risks, for example as households are advised to shut windows to keep outdoor wildfire smoke from getting inside, while simultaneously threatened by high indoor temperatures when lacking air conditioning.

Timely warnings were issued throughout the region by the US National Weather Service, Environment and Climate Change Canada and local governments. British Columbia has “Municipal Heat Response Planning”, which gathers information on heat response plans throughout the province., including responses such as increasing access to cooling facilities and distribution of drinking water. In the long-term strategies, changes to the built environment are emphasized (Lubik et al., 2017). Not all municipalities throughout BC have formalized heat response plans, and others have limited planning,

---

[7] https://vancouversun.com/news/local-news/more-than-25-people-have-died-suddenly-in-burnaby-mostly-due-to-the-heat

[8] https://www.cbc.ca/news/canada/british-columbia/heat-wave-719-deaths-1.6088793

[9] https://apnews.com/article/canada-heat-waves-environment-and-nature-cc9d346d495caf2e245fc9ae923adae1

[10] https://www.seattletimes.com/seattle-news/weather/pacific-northwests-record-smashing-heat-wave-primes-wildfire-buckles-roads-health-toll-not-yet-known

[11] https://globalnews.ca/news/7994540/flooding-record-breaking-heat-rapid-snow-melt-bc-video/

[12] https://www.washingtonpost.com/world/2021/07/01/lytton-canada-evacuated-wildfire-heatwave/

thought to be due to low heat risk perceptions throughout the area, as well as a lack of local data for risk assessments (Lubik et al., 2017).

The extremely high temperatures featured in this heat episode meant that everyone was vulnerable to its effects if exposed for a significant period of time. Although extreme heat affects everyone, some individuals are even more vulnerable, including the elderly, young children, individuals with pre-existing medical conditions, socially isolated individuals, homeless people, individuals without air-conditioning, and (outdoor) workers (Singh et al., 2019). Throughout Seattle's King County the number of vulnerable people is increasing as senior populations continue to rise (DeLaTorre & Neal, 2014; Washington State Department of Social and Health Services, 2019). In addition, Seattle's King County contains the third-largest population of homeless in the U.S, with the numbers increasing during the past decade (Stringfellow and Wagle, 2018). This group largely depends on governmental authorities to provide for sufficient and nearby cooling centers, and governmental authorities have done so by opening several cooling centers throughout Seattle, Portland, and Vancouver BC during the June 2021 heatwave. [13] [14] [15] In addition, electrolytes, food, and water were distributed to the homeless.[16] Governmental websites provided information on how and where to stay cool. Analyses will determine whether the numbers of centers were sufficient.

The lack of air conditioning is a significant factor contributing to heat risk. The Pacific Northwest has lower access to air-conditioned homes and buildings compared to other regions in the U.S., with the Seattle metropolitan area being the least air-conditioned metropolitan area of the United States (<50% air conditioning in residential areas) (U.S. Census Bureau, 2019). Portland and Vancouver also have comparably low percentages of air-conditioned households, 79% and 39% respectively (BC Hydro, 2020; U.S. Census Bureau, 2019). Still, a trend towards an increasing percentage of air conditioned homes is being observed in all three cities over the past years and this trend is expected to continue (ibid.).

Current estimates of the population health impacts of the event underestimate how many people died from the heat because of the lag between the event and when death certificates are available. The total mortality impact is determined by quantifying the number of excess deaths, or the numbers of deaths above what is expected for that time of year (without a heatwave). This difference is illustrated by an estimate from the U.S. Centers for Disease Control and Prevention that over the period 2004-2018, 702 Americans died annually from heat-related causes. An estimate of the numbers of excess heat-related deaths in 297 U.S. counties representing 61.9% of the U.S. population for the period 1997-2006 concluded that an average of 5,608 heat-attributable deaths occurred annually (Weinberger et al., 2020). Most deaths in a heatwave do not die from heat stroke but from cardiovascular, respiratory, and other diseases, with heat infrequently noted as a contributing cause on the death certificate.

Recommendations:

Although this extreme heat event is still rare in today's climate, the analysis above shows that the frequency is increasing with further warming. A number of adaptation and risk management priorities that

[13] https://durkan.seattle.gov/2021/06/city-of-seattle-opens-additional-cooling-centers-and-updated-guidance-for-staying-cool-in-extreme-heat%E2%80%AF/
[14] https://www.oregonlive.com/weather/2021/06/portland-cooling-centers-provide-relief-from-heat.html
[15] https://thebcarea.com/2021/06/26/cooling-stations-set-up-around-b-c-for-record-breaking-heat-wave-this-weekend/#comments
[16] https://edition.cnn.com/2021/06/29/weather/northwest-heat-illness-emergency-room/index.html

emerge as the risk of extreme heat continues to rise locally and around the globe. It is crucial that local governments and their emergency management partners establish heat action plans to ensure well coordinated response actions during an extreme heat event - tailored to high-risk groups (Ebi, 2019). Heatwave early warning systems also need to be improved, this includes tailoring messages to inform and motivate vulnerable groups, as well as providing tiered warnings that take into account vulnerable groups may have lower thresholds for risk (Hess and Ebi, 2016). In other words, starting to warn the most vulnerable early as temperatures start to rise, this can include temperatures at which the general population is not yet acutely at risk. In cases where heat action plans and heat early warning systems are already robust, it is important that they are reviewed and updated to capture the implications of rising risks - every five years or less (Hess and Ebi, 2016). Further, heatwave early warning systems should undergo stress tests to evaluate their robustness to temperature extremes beyond recent experience and to identify modifications to ensure continued effectiveness in a changing climate (Ebi et al., 2018).

Data availability

Data are available via the KNMI Climate Explorer.

Validation tables

Table 3. As Table 1 but showing all model validation results.

Model / Observations	Seasonal cycle	Spatial pattern	Sigma	Shape parameter	Conclusion
ERA5			1.70 (1.40 ... 1.90)	-0.200 (-0.500 ... 0.00)	
GFDL-CM2.5/FLOR historical-rcp45 (5)	good	good	2.01 (1.84 ... 2.17)	-0.201 (-0.272 ... -0.144)	reasonable, include as different experiment than most other models
ACCESS-CM2 historical-ssp585 (2)	good	good	1.86 (1.71 ... 2.02)	-0.200 (-0.260 ... -0.120)	good
ACCESS-ESM1-5 historical-ssp585 (2)	good	good	2.69 (2.49 ... 2.90)	-0.240 (-0.290 ... -0.190)	bad
AWI-CM-1-1-MR historical-ssp585 (1)	good	good	1.50 (1.35 ... 1.69)	-0.200 (-0.280 ... -0.110)	good
BCC-CSM2-MR historical-ssp585 (1)	good	good	2.22 (2.00 ... 2.49)	-0.230 (-0.310 ... -0.140)	bad
CAMS-CSM1-0 historical-ssp585 (1)	good	good	1.98 (1.79 ... 2.23)	-0.200 (-0.290 ... -0.100)	reasonable, exclude because enough good CMIP5 models
CMCC-CM2-SR5 historical-ssp585 (1)	good	good	1.29 (1.15 ... 1.46)	-0.0800 (-0.160 ... 0.0300)	reasonable, exclude because enough good CMIP5 models
CNRM-CM6-1 historical-ssp585 (1)	good	good	1.54 (1.39 ... 1.72)	-0.210 (-0.290 ... -0.100)	good
CNRM-CM6-1-HR historical-ssp585 (1)	good	good	1.48 (1.33 ... 1.66)	-0.190 (-0.270 ... -0.100)	good
CNRM-ESM2-1	good	good	1.71 (1.54 ... 1.92)	-0.180 (-0.250 ...	good

historical-ssp585 (1)				-0.0900)	
CanESM5 historical-ssp585 (50)	good	reasonable	1.79 (1.76 ... 1.82)	-0.180 (-0.190 ... -0.170)	reasonable, include because statistical parameters good
EC-Earth3 historical-ssp585 (3)	good	good	1.87 (1.76 ... 2.00)	-0.220 (-0.270 ... -0.170)	good
EC-Earth3-Veg historical-ssp585 (4)	good	good	2.07 (1.95 ... 2.19)	-0.250 (-0.290 ... -0.210)	bad
FGOALS-g3 historical-ssp585 (3)	good	reasonable	1.80 (1.69 ... 1.92)	-0.180 (-0.210 ... -0.140)	reasonable, include because statistical parameters good
GFDL-CM4 historical-ssp585 (1)	good	good	1.43 (1.29 ... 1.62)	-0.210 (-0.300 ... -0.110)	good
GFDL-ESM4 historical-ssp585 (1)	good	good	1.37 (1.23 ... 1.55)	-0.170 (-0.260 ... -0.0700)	reasonable, exclude because enough good CMIP5 models
HadGEM3-GC31-LL historical-ssp585 (4)	good	good	2.00 (1.90 ... 2.12)	-0.210 (-0.250 ... -0.170)	reasonable, exclude because enough good CMIP5 models
HadGEM3-GC31-MM historical-ssp585 (3)	good	good	2.08 (1.96 ... 2.22)	-0.190 (-0.230 ... -0.140)	bad
INM-CM4-8 historical-ssp585 (1)	good	good	1.63 (1.46 ... 1.83)	-0.210 (-0.300 ... -0.110)	good
INM-CM5-0 historical-ssp585 (1)	good	good	1.80 (1.63 ... 2.03)	-0.240 (-0.310 ... -0.140)	good
IPSL-CM6A-LR historical-ssp585 (6)	good	reasonable	1.79 (1.71 ... 1.88)	-0.220 (-0.250 ... -0.180)	reasonable, include because statistical parameters good
KACE-1-0-G historical-ssp585 (3)	good	good	2.27 (2.13 ... 2.41)	-0.241 (-0.282 ... -0.196)	bad
MIROC-ES2L historical-ssp585 (1)	reasonable, peaks about a month early	reasonable	1.46 (1.31 ... 1.65)	-0.190 (-0.300 ... -0.0900)	reasonable, include because statistical parameters good
MIROC6 historical-ssp585 (50)	good	good	1.31 (1.29 ... 1.33)	-0.220 (-0.220 ... -0.210)	bad
MPI-ESM1-2-HR historical-ssp585 (2)	good	good	1.49 (1.39 ... 1.62)	-0.250 (-0.310 ... -0.190)	good
MPI-ESM1-2-LR historical-ssp585 (10)	good	good	1.63 (1.58 ... 1.69)	-0.260 (-0.280 ... -0.230)	good
MRI-ESM2-0 historical-ssp585 (2)	reasonable, peak too flat	good	1.41 (1.30 ... 1.53)	-0.280 (-0.340 ... -0.220)	reasonable, include because statistical parameters good
NESM3 historical-ssp585 (1)	good	good	1.48 (1.34 ... 1.67)	-0.290 (-0.370 ... -0.200)	good
NorESM2-MM historical-ssp585 (1)	good	good	1.90 (1.70 ... 2.12)	-0.250 (-0.350 ... -0.140)	in between reasonable and good, include
UKESM1-0-LL historical-ssp585 (5)	good	good	1.99 (1.90 ... 2.09)	-0.170 (-0.190 ... -0.140)	reasonable, exclude because enough good CMIP5 models
IPSL-CM6A-LR historical-ssp245 (32)	good, from CMIP6	reasonable, from CMIP6	1.69 (1.64 ... 1.75)	-0.220 (-0.250 ... -0.200)	reasonable, obs covar used, different from CMIP6 as different ssp scenario. Use both
GFDL-AM2.5C360 historical (5)	good	good	2.15 (1.99 ... 2.30)	-0.259 (-0.335 ... -0.197)	bad, variability too high

CAM5-1-1degree C20C historical (99)	NA	NA	1.70 (1.68 ... 1.72)	-0.176 (-0.172 ... -0.180)	good, values used with warming level 1.7
MIROC5 C20C historical ()	NA	NA	1.36 (1.33 ... 1.39)	-0.240 (-0.224 ... -0.256)	bad
HadGEM3-A-N216 C20C historical ()	NA	NA	2.00 (1.95 ... 2.05)	-0.240 (-0.218 ... -0.262)	bad

References

Baldwin, J. W., Dessy, J. B., Vecchi, G. A., & Oppenheimer, M. (2019). Temporally compound heat wave events and global warming: An emerging hazard. Earth's Future, 7. https://doi.org/10.1029/2018EF000989.

Barnes, E.A. and J.A. Screen: The impact of Arctic warming on the midlatitude jet-stream: Can it? Has it? Will it? (2015) WIREs Clim Change, 6:277–286. doi: 10.1002/wcc.337.

BC Hydro, (2020, August). Not-so well-conditioned: How inefficient A/C use is leaving British Columbians out of pocket in the cold.

Boucher, O., Servonnat, J., Albright, A. L., Aumont, O., Balkanski, Y., Bastrikov, V., ... & Vuichard, N. (2020). Presentation and evaluation of the IPSL‐CM6A‐LR climate model. *Journal of Advances in Modeling Earth Systems*, *12*(7), e2019MS002010.

Chan D, GA Vecchi, W Yang, P Huybers (2021): Improved simulation of 19th- and 20th-century North Atlantic hurricane frequency after correcting historical sea surface temperatures. Sci. Adv. 2021. doi: 10.1126/sciadv.abg6931.

Coumou, D., Lehmann, J. & Beckmann, J. (2015) The weakening summer circulation in the Northern Hemisphere mid-latitudes. Science 348, 324–327 .

Chang, E. K. M., Ma, C., Zheng, C. & Yau, A. M. W. (2016). Observed and projected decrease in Northern Hemisphere extratropical cyclone activity in summer and its impacts on maximum temperature. Geophys. Res. Lett. 43, 2200–2208.

Christidis, N., and Stott, P. A. (2015), Changes in the geopotential height at 500 hPa under the influence of external climatic forcings, *Geophys. Res. Lett.*, 42, 10,798– 10,806, doi:10.1002/2015GL066669.

DeLaTorre, A. K., & Neal, M. B. (2014). Aging and equity in the greater Portland metropolitan region. Connections: Journal of the Coalition for a Livable Future, 12(1), 10–23.

Ebi KL, Berry P, Hayes K, Boyer C, Sellers S, Enright PM, Hess JJ. (2018) Stress Testing the Capacity of Health Systems to Manage Climate Change-Related Shocks and Stresses. Int J Environ Res Public Health. Oct 26;15(11):2370. doi: 10.3390/ijerph15112370. PMID: 30373158; PMCID: PMC6265916.

Ebi, KL (2019), Effective heat action plans: research to interventions, Environ. Res. Lett. 14 122001.

Fetterer, F., K. Knowles, W. N. Meier, M. Savoie, and A. K. Windnagel. (2017, updated daily). Sea Ice Index, Version 3. Ice Extent; Sea Ice Concentration. Boulder, Colorado USA. NSIDC: National Snow and Ice Data Center. doi: https://doi.org/10.7265/N5K072F8. Accessed 2 July, 2021.

Haarsma, R.J., Selten, F. & van Oldenborgh, G.J. (2013). Anthropogenic changes of the thermal and zonal flow structure over Western Europe and Eastern North Atlantic in CMIP3 and CMIP5 models. Clim Dyn 41, 2577–2588. https://doi.org/10.1007/s00382-013-1734-8.

Haines A, Kovats RS, Campbell-Lendrum D, Corvalan C. (2006). Climate change and human health: impacts, vulnerability, and mitigation. Lancet. 2006 Jun 24;367(9528):2101-9. doi: 10.1016/S0140-6736(06)68933-2. Erratum in: Lancet. 2006 Aug 19;368(9536):646. PMID: 16798393.

Hall, A., X. Qu, and J.D. Neelin (2008). Improving predictions of summer climate change in the United States. Geophys. Res. Lett., 35(1), L01702, doi:10.1029/2007GL032012.

Hansen, J., Ruedy, R., Sato, M., and Lo, K. (2010). Global surface temperature change. Rev. Geophys., 48, RG4004, https://doi.org/10.1029/2010RG000345.

Harvey, B.J, P. Cook, L.C. Shaffrey and R. Schiemann (2020). The Response of the Northern Hemisphere Storm Tracks and Jet Streams to Climate Change in the CMIP3, CMIP5, and CMIP6 Climate Models, Journal of Geophysical Research: Atmospheres, 125.

Hauser, M., R. Orth, and S. I. Seneviratne (2016). Role of soil moisture versus recent climate change for the 2010 heat wave in Russia. Geophys. Res. Lett., 43, 2819–2826, doi:10.1002/2016GL068036.

Hersbach, H, Bell, B, Berrisford, P, et al. (2020). The ERA5 global reanalysis. *Q J R Meteorol Soc*., 146: 1999– 2049. https://doi.org/10.1002/qj.3803.

Hess, J.J. and Ebi, K.L. (2016), Iterative management of heat early warning systems in a changing climate. Ann. N.Y. Acad. Sci., 1382: 21-30. https://doi.org/10.1111/nyas.13258

D'Ippoliti et al., (2010). The impact of heat waves on mortality in 9 European cities: results from the EuroHEAT project Environmental Health, 9–37.

Kew, S. F., Philip, S. Y., Hauser, M., Hobbins, M., Wanders, N., van Oldenborgh, G. J., van der Wiel, K., Veldkamp, T. I. E., Kimutai, J., Funk, C., and Otto, F. E. L. (2021). Impact of precipitation and increasing temperatures on drought trends in eastern Africa, Earth Syst. Dynam., 12, 17–35, https://doi.org/10.5194/esd-12-17-2021.

Kirchmeier-Young et al. (2018). Attribution of the influence of human-induced climate change on an extreme fire season, Earth's Future, 7, 2-10, doi:0.1029/2018EF001050.

Kornhuber, K and T. Tamarin-Brodsky, (2021). Future Changes in Northern Hemisphere Summer Weather Persistence Linked to Projected Arctic Warming, Geoph. Res Lett. 48.

Lehmann, J., Coumou, D., Frieler, K., Eliseev, A. V. & Levermann, A. (2014). Future changes in extratropical storm tracks and baroclinicity under climate change. Environ. Res. Lett. 9, 084002.

Lenssen, N., Schmidt, G., Hansen, J., Menne, M., Persin, A., Ruedy, R., and Zyss, D. (2019). Improvements in the GISTEMP uncertainty model. J. Geophys. Res. Atmos., 124(12), 6307-6326, doi:10.1029/2018JD029522.

Lucie A. Vincent , Megan M. Hartwell & Xiaolan L. Wang (2020): A Third Generation of Homogenized Temperature for Trend Analysis and Monitoring Changes in Canada's Climate, Atmosphere-Ocean, DOI: 10.1080/07055900.2020.1765728.

Lubik, A., McKee, G., Chen, T., & Kosatsky, T. (2017). Municipal Heat Response Planning in British Columbia, Canada 2017.

Menne, M.J., I. Durre, R.S. Vose, B.E. Gleason, and T.G. Houston, 2012: An overview of the Global Historical Climatology Network-Daily Database. Journal of Atmospheric and Oceanic Technology, 29, 897-910, doi.10.1175/JTECH-D-11-00103.1.

Mueller, B., and S.I. Seneviratne, (2012). Hot days induced by precipitation deficits at the global scale. *Proceedings of the National Academy of Sciences*, 109 (31), 12398-12403, doi: 10.1073/pnas.1204330109.

Neale et al. (2010) Description of the NCAR community atmosphere model (CAM 5.0). NCAR Tech. Note NCAR/TN-486+ STR, 1(1), 1-12.

Pfleiderer, P., Schleussner, C.-F., Kornhuber, K. and Coumou, D. (2019). Summer weather becomes more persistent in a 2C world, Nat. Clim. Chang., doi:10.1038/s41558-019-0555-0.

Philip, S., Kew, S., van Oldenborgh, G. J., Otto, F., Vautard, R., van der Wiel, K., King, A., Lott, F., Arrighi, J., Singh, R., and van Aalst, M. (2020). A protocol for probabilistic extreme event attribution analyses, Adv. Stat. Clim. Meteorol. Oceanogr., 6, 177–203, https://doi.org/10.5194/ascmo-6-177-2020.

Routson, CC, N.P. McKay, D.S. Kaufman, M.P. Erb, H. Goosse, B.N. Shuman, J.R. Rodysill & T. Ault (2019). Mid-latitude net precipitation decreased with Arctic warming during the Holocene, Nature, 568, 83-87.

Skamarock, W. C., J. B. Klemp, J. Dudhia, D. O. Gill, Z. Liu, J. Berner, W. Wang, J. G. Powers, M. G. Duda, D. M. Barker, and X.-Y. Huang (2019). A Description of the Advanced Research WRF Version 4. NCAR Tech. Note NCAR/TN-556+STR, 145 pp. doi:10.5065/1dfh-6p97.

Seneviratne, S.I., T. Corti, E.L. Davin, M. Hirschi, E.B. Jaeger, I. Lehner, B. Orlowsky, and A.J. Teuling (2010). Investigating soil moisture-climate interactions in a changing climate: A review. *Earth-Science Reviews*, 99, 3-4, 125-161, doi:10.1016/ j.earscirev.2010.02.004.

Singh, R., Arrighi, J., Jjemba, E., Strachan, K., Spires, M., Kadihasanoglu, A. (2019) 'Heatwave Guide for Cities'. Red Cross Red Crescent Climate Centre.

Stone et al. (2019) Experiment design of the International CLIVAR C20C+ Detection and Attribution Project. *Weather and Climate Extremes*, 24, 100206. https://doi.org/10.1016/j.wace.2019.100206.

Stringfellow & Wagle (2018, May 18). The Economics of Homelessness in Seattle and King County. McKinsey & Company. Retrieved from: https://www.mckinsey.com/featured-insights/future-of-cities/the-economics-of-homelessness-in-seattle-and-king-county. (Accessed on: July 4, 2021).

Tang Q., X. Zhang, and J.A. Francis (2014). Extreme summer weather in northern mid-latitudes linked to a vanishing cryosphere. Nat Clim Change, 4:45–50.

Taylor, K. E., Stouffer, R. J., & Meehl, G. A. (2012). An overview of CMIP5 and the experiment design. Bulletin of the American Meteorological Society, 93(4), 485–498. https://doi.org/10.1175/BAMS-D-11-00094.1.

U.S. Census Bureau (2019). American Housing Survey (AHS). Retrieved from: https://www.census.gov/programs-surveys/ahs/data/interactive/ahstablecreator.html.

Van Oldenborgh, G.J., van der Wiel, K., Kew, S. et al. (2021). Pathways and pitfalls in extreme event attribution. *Climatic Change*, 166**,** 13, https://doi.org/10.1007/s10584-021-03071-7.

Vautard, R., M. van Aalst, O. Boucher, A. Drouin, K. Haustein, F. Kreienkamp, G.-J. van Oldenborgh, F. E. L. Otto, A. Ribes, Y. Robin, M. Schneider, J.-M. Soubeyroux, P. Stott, S. I. Seneviratne, M. Vogel, M. Vavrus, S.J. (2018). The Influence of Arctic amplification on mid-latitude weather and climate. Curr. Clim. Change Rep. 4, 238–249.

Vecchi, G. A., Delworth, T., Gudgel, R., Kapnick, S., Rosati, A., Wittenberg, A. T., & Zhang, S. (2014). On the seasonal forecasting of regional tropical cyclone activity. Journal of Climate, 27(21), 7994–8016. https://doi.org/10.1175/jcli-d-14-00158.1.

Washington State Department of Social and Health Services (2019). Selected Population and Aging Service Utilization Forecast, King County Aging & Disability Services. Retrieved from: https://www.dshs.wa.gov/altsa/stakeholders/aging-demographic-information. (Accessed on: July 3, 2021).

Wehner (2019). Human contribution to the record-breaking June and July 2019 heat waves in Western Europe, *Environ. Res. Lett.*, https://iopscience.iop.org/article/10.1088/1748-9326/aba3d4/pdf.

Weinberger KR, Harris D, Spangler KR, Zanobetti A, Wellenius GA. (2020). Estimating the number of excess deaths attributable to heat in 297 United States counties. Environ Epidemiol. 2020 Apr 23;4(3):e096. doi: 10.1097/EE9.0000000000000096. PMID: 32613153; PMCID: PMC7289128.

Wehrli, K., Guillod, B. P., Hauser, M., Leclair, M., Seneviratne, S. I. (2019). Identifying key driving processes of major recent heat waves. Journal of Geophysical Research: Atmospheres, 124. https://doi.org/10.1029/2019JD030635.

Yang W, TL Hsieh, GA Vecchi (2021): Why is the Hurricane Season So Sharp? EarthArXiv 2021. doi: 10.31223/X5Q31B.